Università Politecnica delle Marche
Scuola di Dottorato di Ricerca in Scienze dell'Ingegneria
Curriculum in Ingegneria Meccanica e Gestionale

A new hybrid soft-sensing approach (based on IR Sensor data) for the assessment of the properties characterizing the dynamic thermal behaviour of a building component

Ph.D. Dissertation of:
Antonio D'Antuono

Advisor:
Prof. Gian Marco Revel

XV edition - new series

Università Politecnica delle Marche
Scuola di Dottorato di Ricerca in Scienze dell'Ingegneria
Curriculum in Ingegneria Meccanica e Gestionale

A new hybrid soft-sensing approach (based on IR Sensor data) for the assessment of the properties characterizing the dynamic thermal behaviour of a building component

Ph.D. Dissertation of:
Antonio D'Antuono

Advisor:
Prof. Gian Marco Revel

XV edition - new series

Università Politecnica delle Marche
Dipartimento di Ingegneria Meccanica e Scienze Matematiche
Facoltà di Ingegneria
Via Brecce Bianche — 60131 - Ancona, Italy

Acknowledgements

First of all, I wish to thank my parents. Once again their help was vital in this experience. And thanks to my family, my brothers for all the moments together, unfortunately not too many in the last years.

I wish to thank the reviewers, Jürgen Frick and Gianluca Rossi, for their helpful comments.

Thanks to my advisor, Professor Gian Marco Revel, for the availability and the excellent advices he gave me during these years.

Thanks to Professor Nicola Paone, my scientific tutor for a part of the PhD course, and Professor Enrico Primo Tomasini.

Thanks to Milena Martarelli and Giuseppe Pandarese for having supported and helped me constantly with great advices during my training.

Many thanks to Professor Paolo Castellini and Paolo Chiariotti as far as I could learn by working alongside them.

Thanks to Claudio Santolini and Savio Evangelisti for their support in this years.

Thanks to the guys who have shared with me this path not only from the business point of view, Lorenzo, Fede, Luigi, Bud, Claudio, Giampi, Edo, Marco E., Marco A., Alfo, Livia, Sara, Gloria, Rachele, Luigi C., Filippo, Andrea, Matteo F., Elisa, Matteo B. Many beautiful friendships were born in these three years.

Thanks to my "house mates", Michele, Ago, Ale, Giamma, Elisa and Gianluca for the wonderful time spent together.

Thanks to my friends, Save & Cate, Pitch & Giusy, Raf, Angelo & Fra, Ste & Pam, Anto & Milica. Despite the distance we can always make us some laughs together.

Last, but not least, thanks to you Stefania! this last year was amazing with you. Thanks for supporting me in all the moments. You are amazing and I am really lucky to have you with me.

Thanks also to Birba…for the scratches and the sleepless nights.

Abstract

The critical mass of Energy-efficient Buildings (EeB) in Europe by 2020 will be achieved through sustainable industrialization of high-performance architectural, structural and building-service components. However, realizing the targeted performance in design is hampered by critical shortcomings during on-site construction and refurbishment that cause a lower built-quality and sub-optimal energy-saving in the building lifecycle.

One of the main aspects in terms of energy-saving is related to the thermal performances of the building component. For this reason, more and more works can be found in the literature concerning the thermal properties assessment of the building components (conductivity, thermal transmittance, phase shift).

Many works and standards describes the steady-state condition for the thermal properties evaluation but in more condition, like in-situ application, these conditions are very difficult to reproduce.

For this reason, the research has been focused on the dynamic thermal behavior of a material that allows to characterize the dynamical thermal properties in more reproducible conditions.

The actual methodologies for the dynamic thermal behavior assessment present many problems and difficulties:

- Contact sensors: the actual standards provide a single point evaluation which is not representative of the wall thermal dynamic behavior;
- Environmental conditions: one of the main aspect in terms of measurement uncertainty is represented by the environmental conditions which affect the measured data. In fact, the high sensitivity of the sensors (heat flow meter and thermocouples) makes this aspect critical in a test campaign;
- Time consuming: the actual standards require at least 72h of monitoring for in-situ test. In many conditions there is not the possibility to have a so long time monitoring.

In order to enhance the state-of-the-art, in this document an innovative approach is presented, with the ambition to improve the actual measurement methodologies in terms of accuracy, time-consuming and evaluation of the real building component behavior.

This approach, called Hybrid Soft-Sensing, combines the measurement data and an analytical predictive model in order to evaluate the dynamic thermal behavior of a material by reducing the high level of uncertainty of the actual methodologies and the time consuming for the evaluation.

The approach is based on an optimization loop that compare the wall surface temperature acquired and the obtained one from the analytical model. Furthermore, the data are acquired with an IR sensor that gives the following advantages:

- Non-contact sensor in respect to the actual standards based on the use of thermocouples and heat flow meters;
- Full-field evaluation in respect to a single point evaluation obtained with a contact sensor;
- Less complex and more useful device.

The work flow described in this document can be divided in three different phases:

- Phase I: implementation and validation of the method in a simple case study;
- Phase II: uncertainty and sensitivity evaluation and validation of the model in a more complex case study;
- Phase III: application of the model for the full-field evaluation of the thermal properties and for the overall thermal transmittance assessment of the envelope.

The results obtained show a deviation between the declared value of thermal transmittance of the building component analyzed less than 1 % and a reduction in terms of the time consuming. In fact, the actual standards require more than 72h for an accurate evaluation while the developed Soft-Sensing method requires a time comparable to the phase of the material.

A Monte Carlo analysis has been conducted in order to evaluate the uncertainty of the methodology, in accordance with the GUM, and gives a result less than ±4 %.

Furthermore, a sensitivity analysis has been conducted on the environmental conditions (air velocity and radiative external source) that affect the methodology with an uncertainty result up to 5% in more unfavorable conditions.

This result enhances the actual standard procedures that have a declared uncertainty value of ±8 % for the heat flow meter method and up to ±20 % for the IR sensor method.

The method proposed in the document needs a more complex validation case, in order to make the methodology applicable in in-situ conditions.

Future works could be able to improve the methodology enhancing the boundary conditions assessment that increase the method's uncertainty. The regressive model

approach could be the right way to reduce the dependencies of the acquired data to the environmental noise condition (like external radiation or convective effects).

Contents

List of Figures

List of Tables

List of Acronyms and abbreviations

- *SL*: Single layer panel;
- *DL*: Double layer panel;
- *EPS*: Expanded Polystyrene;
- *XPS*: Extruded Polystyrene;
- *E*-SL: Single layer EPS panel;
- k: Thermal Conductivity in W m^{-1} K^{-1};
- ρ: Density in kg m^{-3};
- ϕ: Phase in s;
- c_p: Specific Heat in J kg^{-1} K^{-1};
- U: Thermal transmittance in W m^{-2} K^{-1};
- C: Thermal conductance in W m^{-2} K^{-1};
- *ETTV*: Envelope Thermal Transfer Value;
- δ: Discrepancy;
- *TC*: Thermocouple;
- *HF*: Heat Flow meter;
- $T_{w,meas}$: Surface temperature on measurement side;
- $T_{air,meas}$: Air temperature on measurement side;
- $T_{w,load}$: Surface temperature on load side;
- $T_{air,load}$: Air temperature on load side;
- $T_{w,meas\ IR}$: Surface temperature on measurement side acquired by IR sensor;
- T_{ref}: Reflected temperature;
- h_r: Radiative heat transfer coefficient;
- h_c: Convective heat transfer coefficient;
- σ: Constant of Stefan-Boltzmann (5.67e^{-8} W m^{-2} K^{-4});
- ε: Emissivity.

Chapter 1

Introduction

In the recent years more and more attention has been given on the energy-saving and emissions reduction. Furthermore, the built environment affects the life and work of all citizens.

The construction sector also has a crucial impact on the EU environment and energy policies as buildings use 40 % of total EU energy consumption and responsible for 36 % of Green-House Gases in Europe while the replacement rate of the existing stock is very small (1-2 % per year).

The buildings sector is on the critical path to decarbonise the European economy by 2050 in line with the Energy Union Strategy. In order to achieve this objective, it must enable reducing its CO2 emissions by 90 % and its energy consumption by as much as 50 %. In this way, the construction and building sector will support the implementation of the COP21 Paris Agreement and contribute to the UN's Sustainable Development Agenda for 2030, including SDG 13 'Take urgent action to combat climate change and its impacts' [1].

The European commission funds every year many research projects about these fundamental aspects.

The work described in this document is contextualized in one of these project called INSITER (*Intuitive Self-Inspection Techniques using Augmented Reality for construction, refurbishment and maintenance of energy-efficient buildings made of prefabricated components*) [2] approved and funded in the call "H2020-EeB-2014-2015 / EeB-03-2014" of the European research program Horizon 2020.

In particular, this document describes an innovative methodology developed for the thermal performance assessment of a construction component.

The main aspect in terms of thermal performances of a building component is the thermal transmittance of the object that represents the component capability to exchange heat with the surrounding environment. For this reason, the knowledge of this parameter during the design phase of a building has a main importance and it has to be measured after the building envelope construction in order to verify its agreement with the value estimated at the design stage.

Several standards, which are reported in bibliography, describe the procedures for the thermal transmittance assessment in both lab and in-situ, however some drawbacks have been identified in such methods:

- the use of contact sensors (as thermal flow meters) that cannot be applied in finished building element;
- the duration of the tests that must be at least 72 hours;
- the low level of accuracy due to the strong dependence to environmental conditions variability.

The first drawback can be overcome by using non-contact sensors such as IR thermal camera, which has been often applied in the past also in the building sector. However, the measurement inaccuracy can increase up to 20 %, as stated in [3]. The inaccuracy of experimental methods and the duration of the tests can be drastically reduced if the tests are accompanied by the use of predicted models. This kind of approach is called Soft-Sensing, which is a combination of the words "software", which is the basis of numerical models, and "sensors", because sensors are used to acquire experimental data used to validate and integrate numerical data, estimated by the model.

Common effects present in the experimental data as measurement noise, missing values, data outliers, co-linear features and varying environmental conditions can be solved by integrating those data with the ones coming from the model thus helping increasing the accuracy and reduce testing time.

1.1 State-of-the-art

There are different standards [4], [5] and [6] for the thermal transmittance assessment, as shown in the Figure 1, related to different test case conditions (laboratory test, in-situ test).

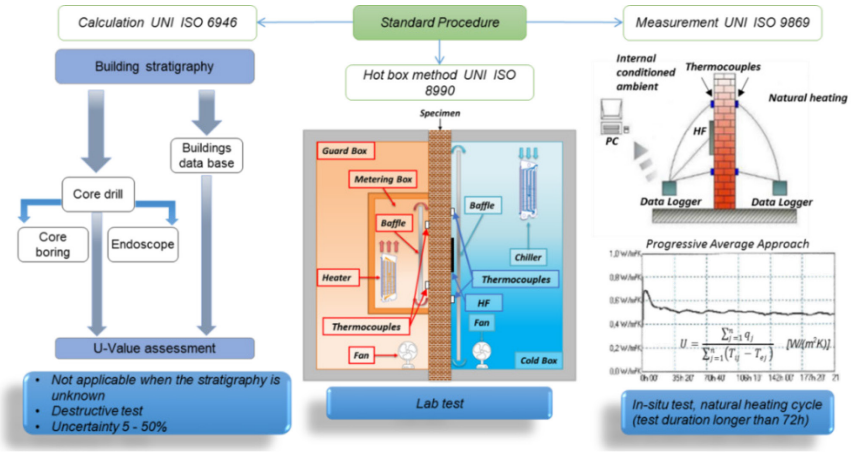

Figure 1. Overview of the current standards for thermal transmittance assessment

- *ISO 6946* [4]: this standard defines the thermal transmittance assessment by knowing the stratigraphy of the building component. For this reason, it represents a destructive method (core boring or endoscopic test is required) with a high level of inaccuracy (5-50 %);
- *ISO 8990* [5]: laboratory test for the thermal transmittance assessment. Based on thermal contact sensors (heat flow meter and thermometer) and on a steady-state thermal condition (long time required).
- *ISO 9869* [6]: in-situ test based on thermal contact sensors (heat flow meter and thermometer). The data acquired during the test must be post-processed with a progressive average method in order to reduce the uncertainty related to casual effects in the environmental conditions (radiative and convective effects). The final value obtained is affect by un uncertainty value greater than 8 %.

Those standards do not consider the dynamic thermal behavior of the building component, which is very important for the thermal transmittance assessment by means of in-situ test, because in this kind of test is almost impossible to obtain a steady-state condition for the thermal transmittance assessment.

For this reason, in the literature many works based on the evaluation of the dynamic thermal behavior of the component can be found.

One of the more robust and reliable method is the Thermal Admittance method that represents the actual state-of-the-art in terms of dynamic behavior prediction of a building component. This method is already defined by the international standard ISO 13786 [7] and used in the standards ISO 13791 [8] and ISO 13792 [9].

Many works based on this approach were found in the literature [10], [11] and [13]. The limitation of this method is related to its formulation based on the knowledge of the thermal properties of the material.

An enhancement in respect to the method described before is represented by the work [13] that reduces the number of thermal properties known by introducing a numerical simulation able to understand some material characteristic by matching the obtained results with the obtained one by the experimental test.

Others recent works describes the thermal transmittance measurement in in-situ test with heat flow transducer [14] and focus their attention on the influence of environmental conditions on this measurement [15]

The methodologies described before are strongly connected to long time consuming experimental tests based on contact sensors. A non-contact sensor approach based on the use of a IR sensor is described in the work [3] based on the energy balance between conduction through the material and convection/radiation caused by the surrounding environment but presents an accuracy up to 20 % in the thermal transmittance evaluation. Other works were found in the literature based on the same approach [16], [17] but based on steady-state environmental conditions, very difficult to achieve in in-situ measurement.

1.2 Literature review

The methodology proposed in this document has a very similar approach in respect to the work of Pernigotto et al. [13], with the main advantage of being less time consuming, approximatively the phase of the component in respect to the other works that require at least 72 h of monitoring. Besides, it is not required to know in advance the building element thermal conductivity.

This method is based on the integration between experimental data, measured by an IR camera and numerical data estimated by an analytical model, which is a hybrid method that can be called Soft Sensing. The measured data are used as input of a software optimization loop based on finding the minimum mean square deviation between the measured and predicted temperature by the model on the surface of the component opposite in respect to thermal load.

1.3 Document overview

This document describes the different phases of the development of the proposed methodology.

In sections 2 and 3 the development and the validation of the method on a simple case study are shown.

In sections 4 the uncertainty of the method has been evaluated by following the international standard GUM and a sensitivity analysis has been conducted on the critical environmental conditions (air velocity, emissivity and radiative source) that affects the method results.

Finally, in section 5, the application of the method to a more complex case study is reported.

The Appendix A describes the application of the method in order to evaluate the total building envelope energy performance and the energy consumption related to the overall thermal transmittance of the building envelope.

The structure of the thesis can be illustrated by the flow-chart reported in Figure 2.

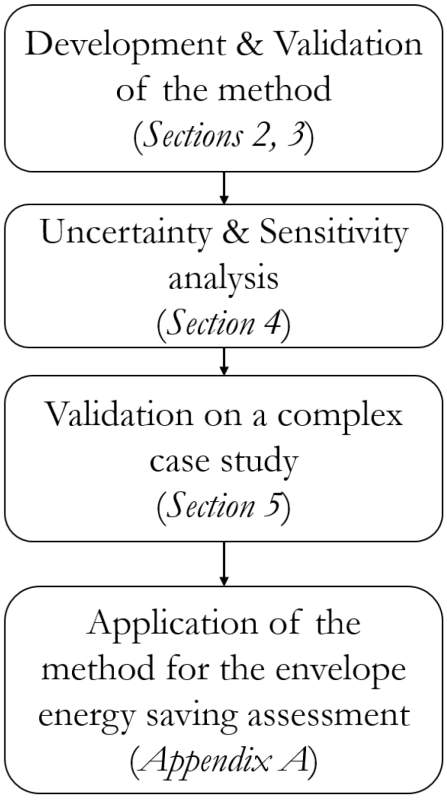

Figure 2. Flow chart of the development, validation and application of the method

Chapter 2

Methodology

The methodology proposed to enhance the actual state-of-the-art in terms of accuracy and time saving for the thermal performances assessment is based on a hybrid Soft-Sensing approach that combines experimental data (measured by sensors) with synthesized ones (predicted by simulation software and specifically analytical models of the thermal dynamic behavior of the component).

In this chapter, the analytical model developed will be presented and its validation through experimental test will be discussed. The results of the analytical model have been also compared with the ones of a FE model of the same component.

2.1 Analytical model

The analytical model exploited in the Soft-Sensing method allows predicting the surface temperature of the building component under test and optimizing the thermal properties governing the dynamic behavior of the component itself, by comparing that calculated and measured temperatures through an optimization algorithm.

The analytical model is based on the equation describing the conductive, convective and radiative phenomena involved in the heat transfer process across a component [18].

In a homogeneous and not defected component, the heat transfer process is governed by conduction (through the component thickness), radiation and convection (at the boundaries of the component) phenomena that are expressed by the heat flow across the component thickness (y-direction) and energy balance at the boundaries.

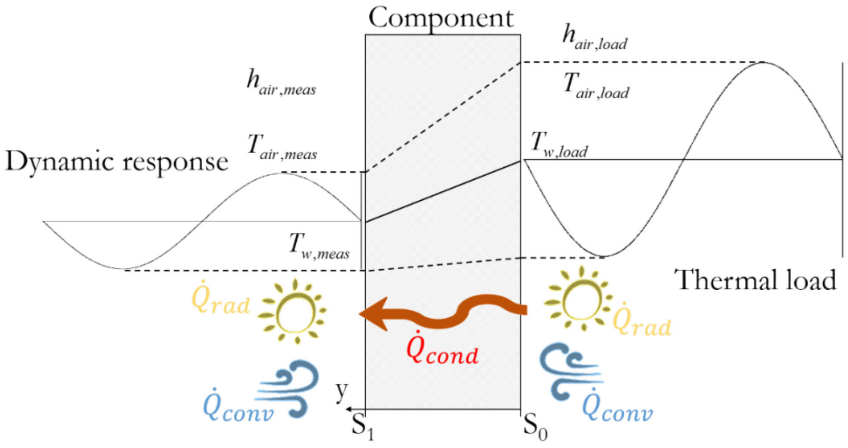

Figure 3. Thermal dynamic behavior of a component

In the Figure 3 the dynamic thermal behavior of a generic component is presented. The physical and geometrical quantities governing the conductive, convective and radiating phenomena are:

- $T_{w,meas}$, surface temperature at the response side of the component, where the measured and calculated temperatures will be compared for the optimization
- $T_{air,meas}$ air temperature at the response side of the component
- $T_{w,load}$ surface temperature at the load side of the component, where the thermal load is applied
- $T_{air,load}$ air temperature at the load side of the component
- $h_{air,meas}$ heat transfer coefficient of the response side
- $h_{air,load}$ heat transfer coefficient of the load side
- $\dot{Q}_{cond}$ conductive heat flow across the component in y-direction
- $\dot{Q}_{conv}$ convective heat flow at the boundaries
- $\dot{Q}_{rad}$ radiative heat flow at the boundaries
- S_0 surface of thermal exchange at the load side
- S_1 surface of thermal exchange at the response side.

The total heat flow is defined by Equation (1) [19].

$$\dot{Q}_{cond} = \dot{Q}_{conv} + \dot{Q}_{rad} \left[\frac{W}{m^2} \right] \tag{1}$$

where $\dot{Q}$ is the total heat flow K is the total heat transfer coefficient in W m^{-2} K^{-1}.

2.1.1 Conduction

The stationary heat conduction through the opposite surfaces of a sample is governed by Fourier's Law, Equation (2) [18].

$$\dot{Q}_{cond} = -kA\nabla T = -kA(T_{w,meas} - T_{w,load})\left[\frac{W}{m^2}\right] \qquad (2)$$

where k is the thermal conductivity in W m^{-1} K^{-1}. The thermal conductivity is expressed as the quantity of heat transmitted per unit time, t, per unit area, A, and per unit temperature gradient.

2.1.2 Convection

The convective heat flow represents the heat transfer from surface of wetted area A and temperature T_s, to a fluid with a temperature T_∞, in accordance with the Newton's law of cooling, Equation (3). [18]

$$\dot{Q}_{conv} = h_c(T_s - T_\infty) = h_c\left(T_{w,meas} - T_{air,meas}\right)\left[\frac{W}{m^2}\right] \qquad (3)$$

where h_c is the convective heat transfer coefficient.

2.1.3 Radiation

The net rate of heat flow, radiated by a body surrounded by a medium at a temperature T_{ref}, the reflected temperature, is given by the Stefan-Boltzmann Law, Equation (4). [18]

$$\dot{Q}_{rad} = 4\sigma\varepsilon A T_{w,meas}^3 (T_{ref} - T_s) = 4\sigma\varepsilon A T_{w,meas}^3 (T_{ref} - T_{w,meas})\left[\frac{W}{m^2}\right] \qquad (4)$$

where σ is the Stefan-Boltzmann constant (5.67e^{-8} W m^{-2} K^{-4}) and ε the body emissivity.

2.1.4 Total heat flow

Considering the energy balance at the component boundaries Equation (1) can be written considering Equations (2), (3) and (4) as shown in Equation (5).

$$\dot{Q} = -kA\nabla T = h_c (T_{w,meas} - T_{air,meas}) + \\ + h_r (T_{ref} - T_{w,meas}) \left[\frac{W}{m^2} \right] \tag{5}$$

Where h_r is the radiative heat transfer coefficient defined by Equation (6), in accordance with the standard EN ISO 6946 [4].

$$h_r = 4\sigma\varepsilon A T_{w,meas}^3 \left[\frac{W}{m^2 K} \right] \tag{6}$$

The standard EN ISO 6946 [4] defines also the surface resistance, R_s, as shown in Equation (7).

$$R_s = \frac{1}{h_c + h_r} \left[\frac{m^2 K}{W} \right] \tag{7}$$

Equation (5) can be written for the boundaries S_0 and S_1 by Equation (8) and Equation (9), respectively:

$$\left(T_{w,load} - T_{air,load}\right) * h_{c0} + \left(T_{ref,load} - T_{w,load}\right) * h_{r0} = \\ - k * \left. \frac{\partial T}{\partial y} \right|_{y=S_0} \left[\frac{W}{m^2} \right] \tag{8}$$

$$\left(T_{w,meas} - T_{air,meas}\right) * h_{c1} + \left(T_{ref,meas} - T_{w,meas}\right) * h_{r1} = \\ - k * \left. \frac{\partial T}{\partial y} \right|_{y=S_1} \left[\frac{W}{m^2} \right] \tag{9}$$

The terms h_{r0} and h_{r1} in the Equations (8) and (9) have been evaluated in accordance with Equation (6). The terms h_{c0} and h_{c1} have been evaluated in accordance with the standard EN ISO 6946 [4], establishing that the convective heat transfer coefficient for indoor surfaces is 2.5 W m^{-2} K^{-1} (for horizontal flow) and the convective heat transfer coefficient for outdoor surfaces is determined by Equation (10):

$$h_c = 4 + 4v \left[\frac{W}{m^2 K} \right] \tag{10}$$

where v = air velocity in m s^{-1}.

The left-hand side of the Equations (8) and (9) represents the convective and radiative heat transfer while the right-hand side is the conductive heat flux component.

This formulation considers the mono-dimensional flow along the component thickness (y-direction) and it is valid if the material constituting the component is homogeneous and transversal flow is negligible. This approach is based on the hypothesis that the conduction across the material has a more important contribution with respect to the convection at the boundary surface. This hypothesis is verified if the dimensionless Biot number is smaller than 0.1, where the Biot number is defined by Equation (11):

$$Bi = \frac{h * L_c}{k} \tag{11}$$

where L_c is the critical length of the component equal to the half of the thickness.

The thermal and mechanical parameters governing the dynamic behavior of the material are thermal conductivity (k in W m^{-1} K^{-1}), density (ρ in kg) and specific heat (c_p in J kg^{-1} K^{-1}). The first one affects the amplitude of the thermal response of the material, their combination affects the slope of the response curve, as shown in Figure 4.

These parameters are linked together by the phase shift of the material in accordance with the standard ASTM-E 2582-07 [20], Equation (12).

$$\phi = \frac{L^2}{\pi\alpha}[s] \tag{12}$$

Where ϕ is the phase shift in s, L the component thickness in m and α the thermal diffusivity in m^2 s^{-1}defined by Equation (13).

$$\alpha = \frac{k}{\rho c_p}\left[\frac{m^2}{s}\right] \tag{13}$$

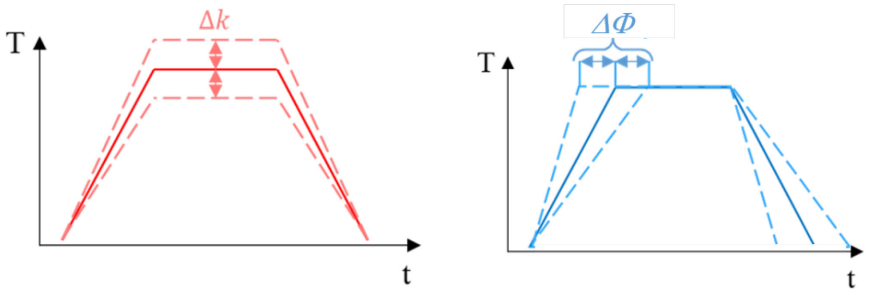

Figure 4. Effect of conductivity (left) and phase (right) on the thermal behavior of the material

Introducing the phase shift in the right-hand side of Equation (9), the conductive contribution of the material to the heat flow across the material is described by the Equation (14).

$$\dot{Q}_{cond}(t) = -k \frac{T_{w,meas}(t) - T_{w,load}(t-\phi)}{L} \left[\frac{W}{m^2}\right] \qquad (14)$$

The result of the analytical model is the surface temperature at the response side obtained by imposing the surface temperature at the load side.

2.2 FE model

The analytical model results (in terms of response side surface temperature) have been compared with the ones of a 2D FE model with the aim to perform a first validation. The FE model has been developed in COMSOL Multiphysics®.
The component analyzed consists of a simple layer of Expanded Polystyrene with certified properties shown in Table 1 and geometry illustrated in Figure 5.

Table 1. Physical properties of the modeled component

Material	Thickness [m]	Conductivity [W m^{-1} K^{-1}]	Density [kg m^{-3}]	Specific Heat [J kg^{-1} K^{-1}]
Expanded Polystyrene	0.03	0.032	30	1450

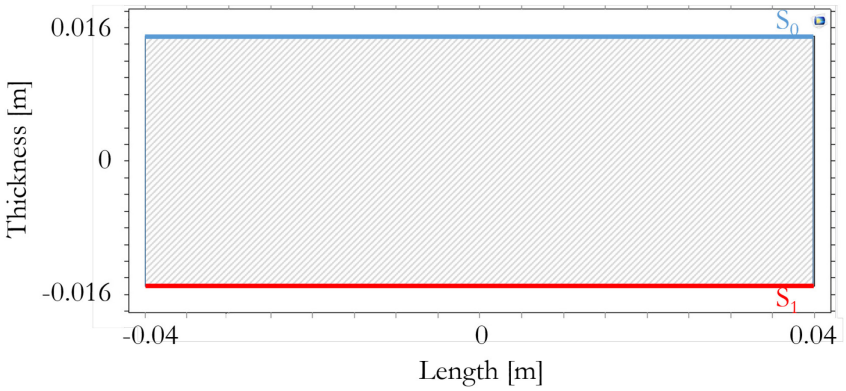

Figure 5. Geometry of the 2D FE model

The model has been developed by using the heat transfer module for solids and fluids. The boundary conditions imposed are reported in Table 2.

Table 2. Boundary conditions

Condition	Geometry level	Equation	Inputs*	Known values**
Conduction	Complete geometry	$L\rho c_p \partial T / \partial t = \nabla \cdot (Lk\nabla T)$	-	
Convection	Boundaries S_0 and S_1***	$-n \cdot (-Lk\nabla T) = Lh \cdot (T_{air} - T)$	$T_{air,load}$ *(for* S_0*)* $T_{air,meas}$ *(for* S_1*)*	h_{c0}, h_{c1},
Insulation	Left and right boundaries	$-n \cdot (-Lk\nabla T) = 0$	-	

*Inputs from experimental test
**Values from the standard
***See Figure 5

2.2.1 FE model validation

The FE model realized has been validated in accordance with the standard EN ISO 10211-1 [21] that defines the calculation of heat flows and surface temperatures within 2D heat transfer models.

The standard defines the tolerance for the validation as follows:

- Temperature: difference between the reference value (from the standard) and calculated one (with the model) less than 0.1 K;
- Flux: difference between the reference value (from the standard) and calculated one (with the model) less than 0.1 W m^{-1}.

The standard indicates 4 different points for the temperature evaluation (points A, B, H and I, marked in red in Figure 6), while the heat flow must be evaluated at the boundary and represents the flow across the component section.
The standard defines also the material constituting the component that consists in a multi-layer panel with external layer in concrete in one side and in aluminum in the other side. The inner layer is an insulation layer and the connection between the aluminum and concrete layers is a wood layer.

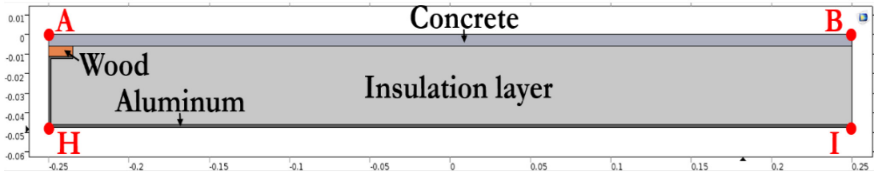

Figure 6. Geometry and materials of the validation model

The model has been evaluated within the following boundaries conditions:

- Top Surface: outdoor ambient with a thermal resistance, R_{se} of 0.04 m^2 K W^{-1} and a temperature of 0 °C;
- Bottom Surface: indoor ambient with a thermal resistance, R_{si} of 0.13 m^2 K W^{-1} and a temperature of 20 °C.

In Figure 7 the temperature profile across the section obtained from the FEM 2D simulation on the model described above is shown.

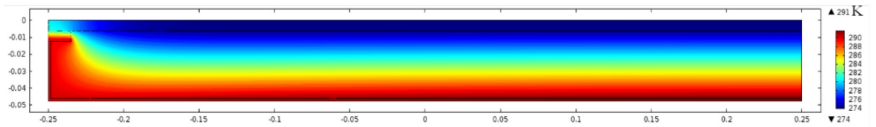

Figure 7. Temperature profile across the model

In Table 3 the results obtained on the control points and the heat flow across the section are shown. A comparison within the value reported in the standard and the one obtained from the FEM simulation are reported in Table 3.

Table 3. Validation in accordance with the standard EN ISO 10211-1 [21].

Quantities	FE models				EN ISO 10211-1				***Discrepancy***			
	A	*B*	*H*	*I*	*A*	*B*	*H*	*I*	***A***	***B***	***H***	***I***
Temperature [K]	7.07	0.76	16.77	18.33	7.1	0.8	16.8	18.3	***<0.1***	***<0.1***	***<0.1***	***<0.1***
Flow [W m^{-1}]	9.495				9.5				***<0.1***			

The results shown in the Table 3 demonstrate that the FE model realized is valid in accordance with the standard and it can be used for the evaluation of the thermal dynamic behavior of any material.

2.2.2 Analytical model validation

In order to validate the analytical model, the surfaces temperature and the heat flow across the panel obtained have been compared with the obtained one from the validated FE model of the panel analyzed (properties in the Table 1).

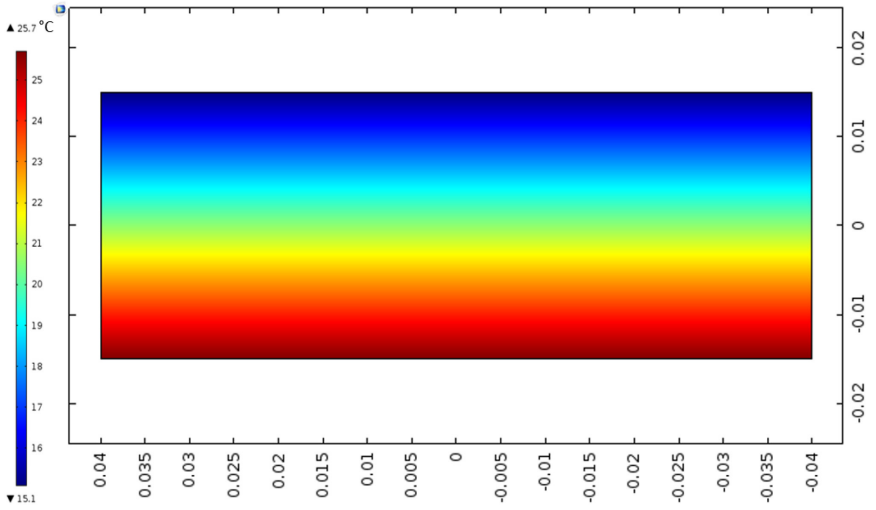

Figure 8. Temperature across the 2D section of the panel

In Figure 8 the results of the FEM simulation on the component is shown. The image shows the temperature distribution across the section of the component.

The comparison between the temperatures on the load side and on the measured side and between the flow across the panel respectively in Figure 9, Figure 10 and Figure 11 is shown.

In Figure 12 the correlation between the data obtained with the FE model and the measured one is presented.

In the figures below the data called *"FEM"* represent the data obtained from the FE model while the data called *"AN"* represent the data obtained from the analytical model.

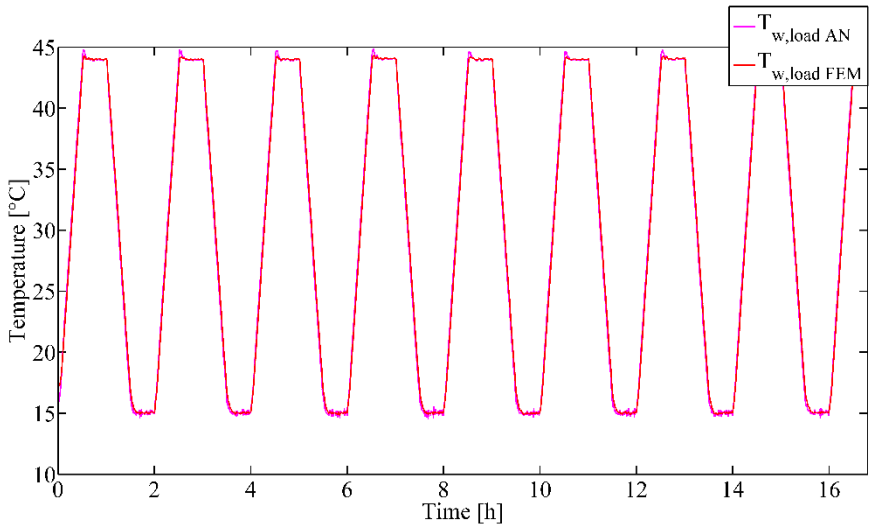

Figure 9. Surface temperature at the load side

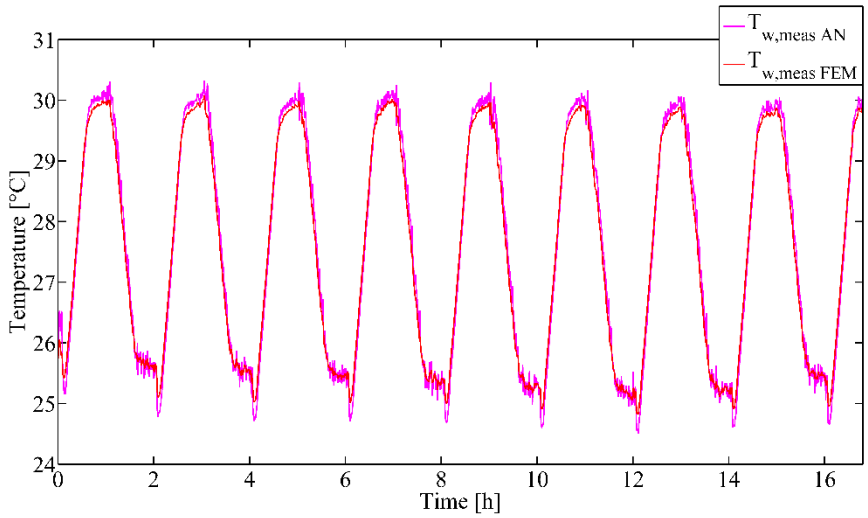

Figure 10. Surface temperature at the response side

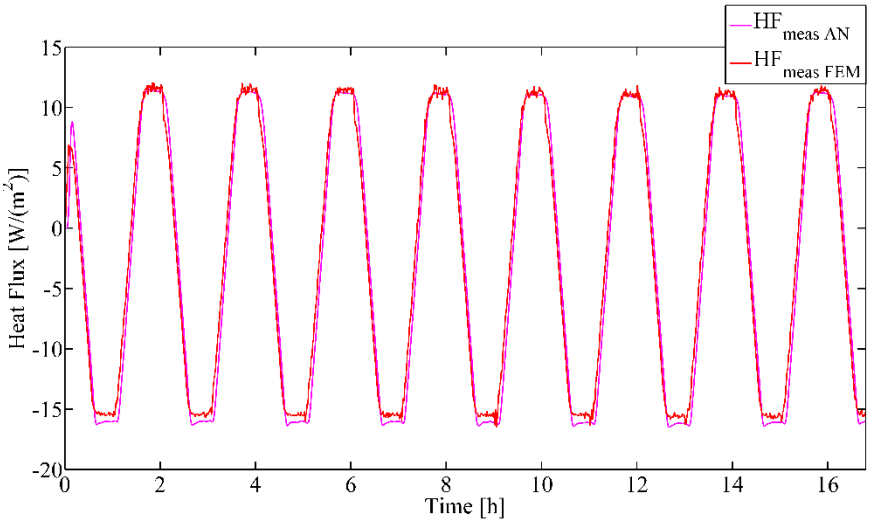

Figure 11. Heat Flux across the panel

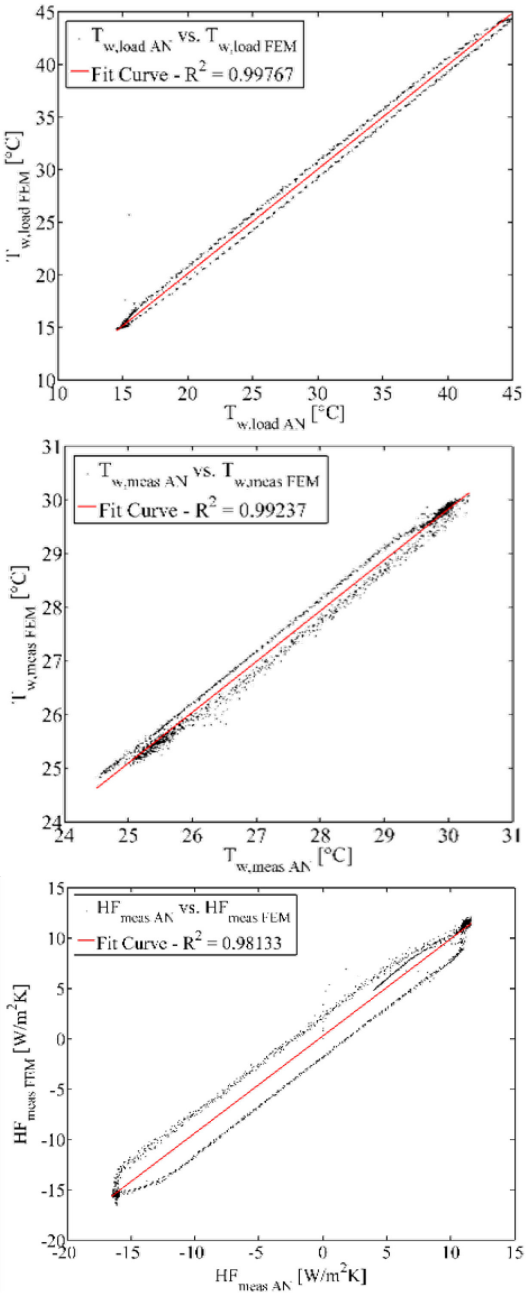

Figure 12. Correlation between analytical and FEM data

The figures above show a good correlation between the experimental and the simulated data. In fact, as shown in the Figure 12, the coefficient of determination R^2, defined by the Equation (18) and defined as a measure of how well observed outcomes are replicated by the model, is at least greater than 0.98.

$$\bar{y} = \frac{1}{n}\sum_{i=1}^{n} y_i \tag{15}$$

Where y_i = measured data; n = total number of data.

$$SS_{tot} = \sum_i \left(y_i - \bar{y}\right)^2 \tag{16}$$

Where SS_{tot} = total sum of squares.

$$SS_{res} = \sum_i \left(y_i - f_i\right)^2 \tag{17}$$

Where SS_{res} = residual sum of squares; f_i = model data.

$$R^2 = 1 - \frac{SS_{res}}{SS_{tot}} \tag{18}$$

The FE model is able to simulate with accurate results the thermal dynamic behavior of a component but the main problem is related to the time required for the calculation. Is known that a FE model requires too much computational time, related to the number of elements forming the mesh of the geometrical model realized.

In this case the model has been discretized by using 30 mesh elements along the thickness and it means that the time required for the simulation is about 10s.

Considering the soft-sensing approach proposed in this work and the necessity of many iteration during an optimization loop, it is easy to understand that a minor expensive method in term of computational time is required.

For this reason, the analytical model has been developed and validated, as shown in the section 2.4.

2.3 Experimental test

Both the analytical and FE models are able to predict the surface temperatures of the component knowing the environmental conditions (air temperatures, air velocity,

radiated temperatures) and the physical properties of the material (conductivity, density and specific heat).

The experimental data to be coupled with the numerical ones have been obtained from a testing campaigned focused on the thermal behavior characterization of a building component simulacrum. The component tested is the one described in section 2 with the physical parameters shown in Table 1.

In Figure 13 the measurement chain is shown.

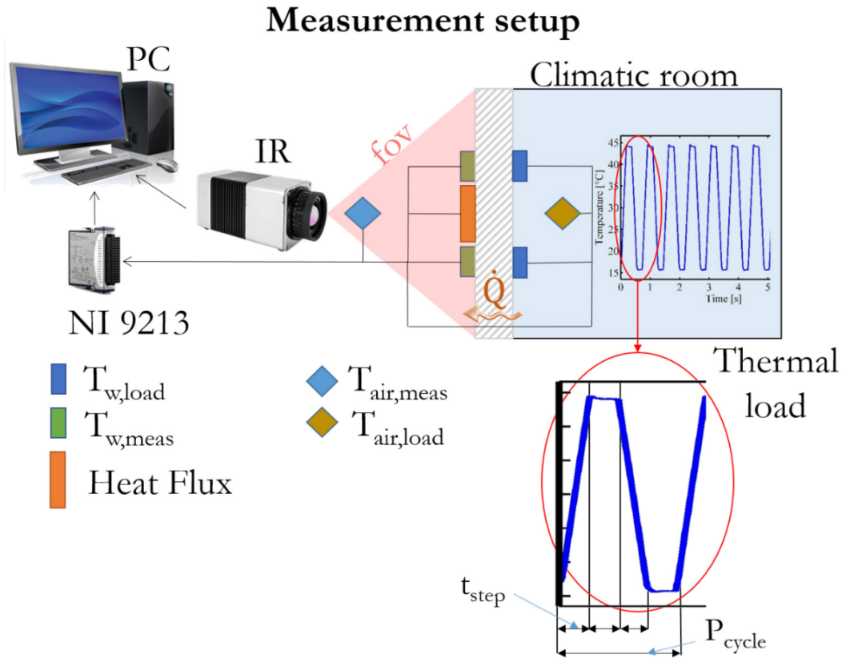

Figure 13. Scheme of the measurement chain

The tests have been made by imposing a thermal load on one side of the panel and monitoring the temperatures and the heat flow through the panel. In detail:

– *Thermal load*: a climatic room has been used to impose a periodical thermal load on one side of the component. The thermal load has been created by controlling the temperature with a trapezoidal cycle between 15 °C and 45 °C. Each step of the trapezoidal load had a duration of 1800s (t_{step}) for a total duration of the cycle

of 2h (P_{cycle}). This cycle has been repeated for 9 times. The panel has been mounted on the climatic room opening.

– *Sensors*: 2 thermocouples have been mounted on each surface of the component to monitor the surface temperature (Tw,meas and Tw,load) and 2 thermocouples have been places indoor and outdoor the thermal camera in order to monitor the environmental air temperature (Tair,meas and T air,load). A heat flux transducer has been mounted on the external surface of the component mounted on the climatic room opening. A thermal camera has been used as non-contact sensor whose output is the temperature of the external surface of the panel (Tw,meas IR). The thermal camera has been placed at 2m from the panel surface in order to a have a field of view (fov) of 1.16m x 0.87m and frame a large portion of the panel where the contact sensors are located.

The data of the thermocouples and the heat flux transducer have been acquired with a National Instruments device (NI 9213), while the thermograms have been recorded by the own made software of the IR camera.
In Table 4 the sensors used for the experimental test and their specifications are shown.

Table 4. Sensors' datasheets.

Tool Type	Model	Specifications
Heat Flux Transducer	Hukseflux – HFP01	Sensitivity: 50 μV/Wm^2 Temperature Range: -30 to 70 °C Sensor Resistance (R): <6.25*10^{-3} m^{2}K/W Accuracy: ±5 %
Thermal Camera	Infratec – Variocam HD	Sensor: Uncooled Microbolometer FPA Spatial Resolution: 1024x768 pixel Spectral Range: 7.5 to 14 μm Temperature Range: -40 to 1200 °C Sensitivity: <0.05 °C Accuracy: ±1.5 °C Frame Rate: 30 Hz
Thermocouple	TCDIRECT – Type T	Materials: Copper vs. Copper-Nickel Temperature Range: -200 to 350 °C Accuracy: ±0.5 °C

Measurement System	National Instruments – NI 9213	Channels: 16 Resolution: 24 bit Measurement Range: ±78.125 mV Accuracy: <0.02 °C

The temperature of the component framed by the IR camera can be recovered from the IR data by applying Equation (19):

$$T_{w,meas} = \sqrt[4]{\frac{T_{cam}^4}{\tau+\varepsilon} - \frac{1-\varepsilon}{\varepsilon} * T_{ref}^4 - \frac{1-\tau}{\varepsilon} * T_{air,meas}^4} \left[K\right] \quad (19)$$

where T_{cam} is temperature measured by the IR sensor and τ is the air transmissivity (≈1).

The reflected temperature has been acquired by using a low-emissivity aluminum sheet attached to the observed surface, see Figure 14.

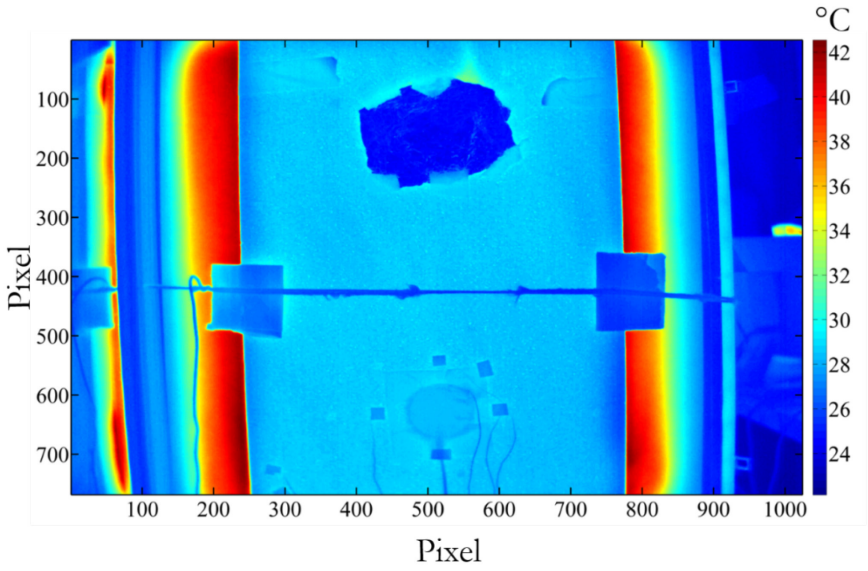

Figure 14. Thermogram of the panel under test

The connection between the panel and the climatic room has been guaranteed with an external frame made in plywood and rubber able to constrain the panel to the

climatic room with a stagnant closure in order to reduce losses in thermal load and undesired air flows.

In Figure 15 the front and rear side of the panel called respectively *meas* and *load* side are shown.

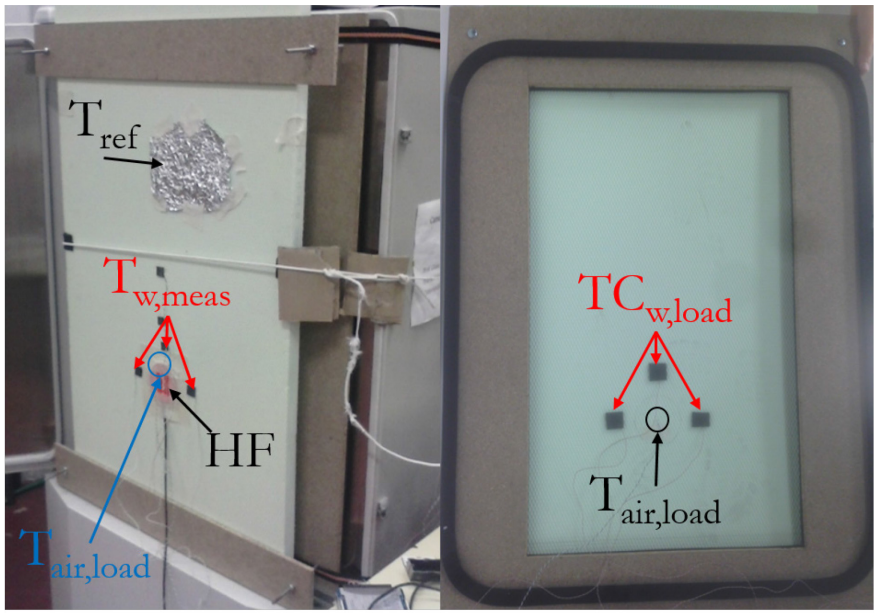

Figure 15. External side (left) and climatic room internal side of the panel under test (right).

In the Figure 16 the complete measurement setup of the test is shown.

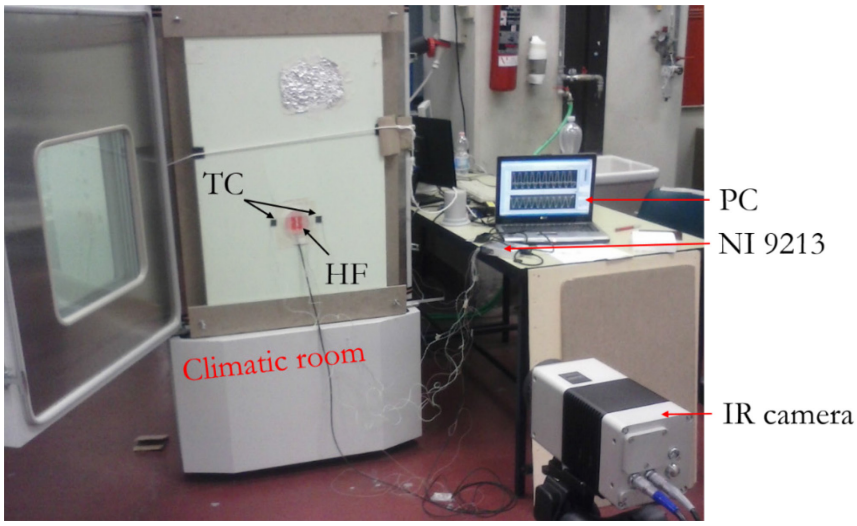

Figure 16. Experimental set-up and view of the front side of the panel (*"meas"*), *TC* indicates the thermocouples location and *HF* the heat flux transducer location

2.4 Results

In Figure 17, Figure 18 and Figure 19 the results are shown.

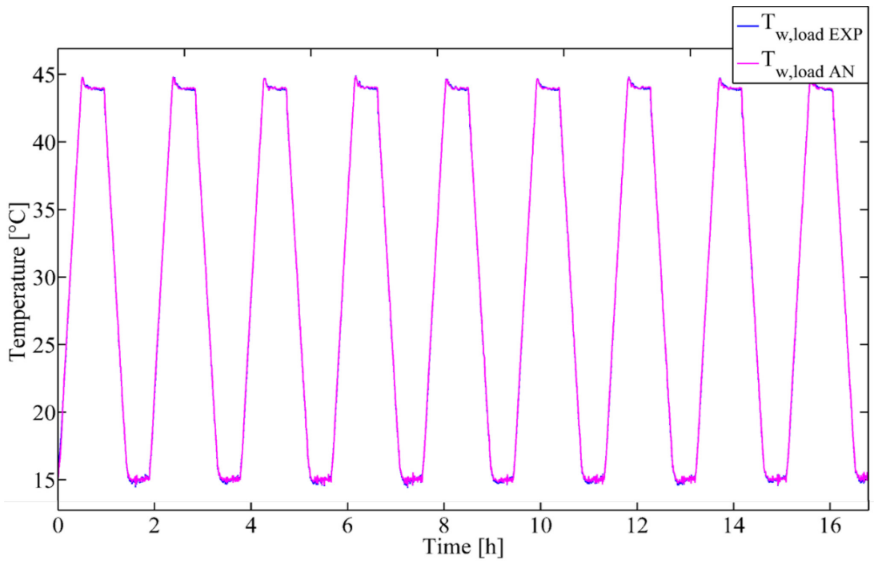

Figure 17. Surface temperature at the load side

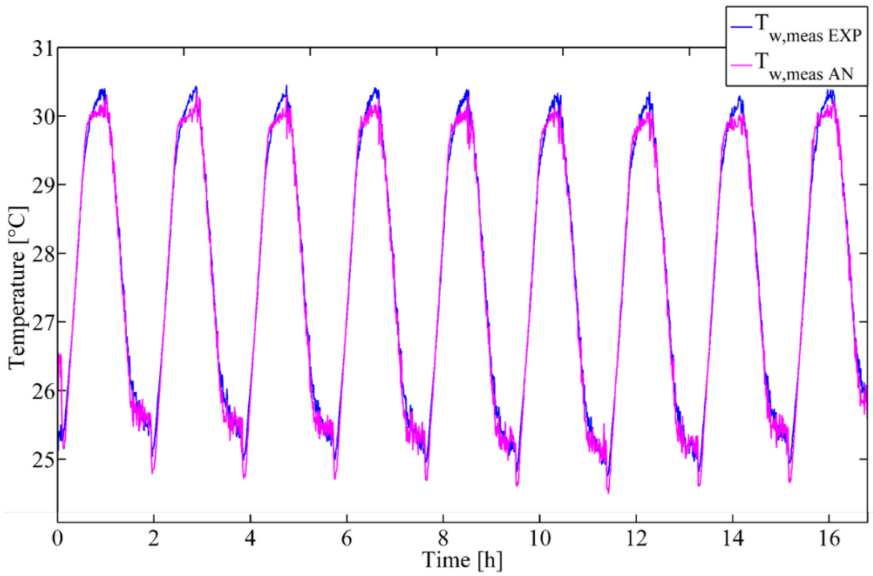

Figure 18. Surface temperature at the response side

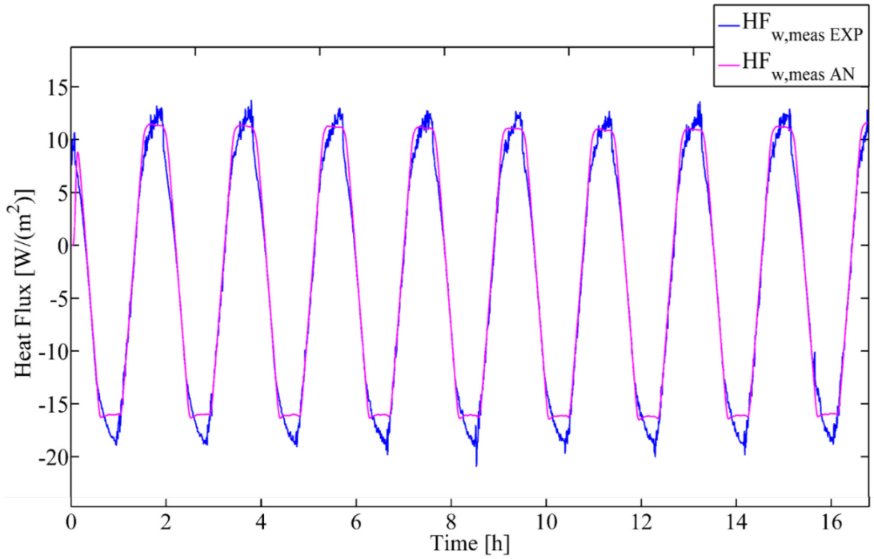

Figure 19. Heat flux across the panel

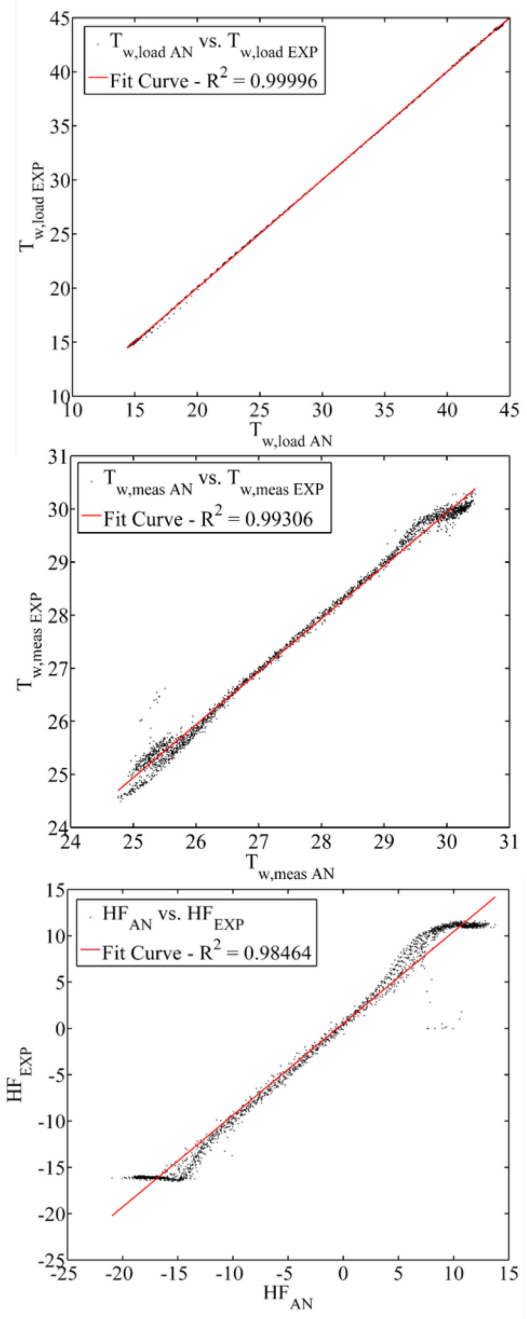

Figure 20. Correlation between experimental and analytical data

In Figure 20 the correlation between the data obtained with the analytical model and the measured one is shown.

The results shown in the figures above shown a high correlation between the experimental data and the data obtained from the analytical model.

In terms of computational time, the analytical model requires less time than the FE model, in fact, the time required is about 0.1s. For this reason, the analytical model is more suitable and effective than the FEM model.

The deviation visible in Figure 19 located at the peaks of the profile is due to the fact that the heat flow transducer has been exposed directly to the environmental air which increases the thermal inertia of the sensor itself.

In Table 5 an overview of the results obtained by comparing the different models used is shown.

Table 5. Results of the comparison between Analytical model and Experimental data.

Model	Coefficient of determination (R^2)			Computational time [s]
	$T_{w,load}$	$T_{w,meas}$	$HF_{w,meas}$	
Analytical	0.993	0.999	0.985	0.1

Chapter 3

Soft-Sensing approach

Once validated the analytical model of the component dynamic thermal behavior, see section 2.1, the Soft-Sensing approach has been developed.

The main idea is to realize an optimization loop able to modify the physical parameters governing the equations describing the dynamic thermal behavior of a material (conductivity, density, specific heat, phase shift).

This method is based on the integration between experimental data, measured by an IR camera and numerical data estimated by the analytical model, which is a hybrid method that can be called Soft Sensing. The measured data are used as input of a software optimization loop based on finding the minimum mean square deviation between the temperature measured experimentally (Tw,meas) and the one predicted by the model at the opposite surface of the component with respect to the thermal load (Tw,an), as shown in Figure 21.

In a first step, the proposed method has been validated with thermal contact sensors (thermocouples and heat flow transducer) and then it has been applied by using experimental data measured by an IR camera, with the advantages of being non-contact and giving a full-field evaluation of thermal transmittance.

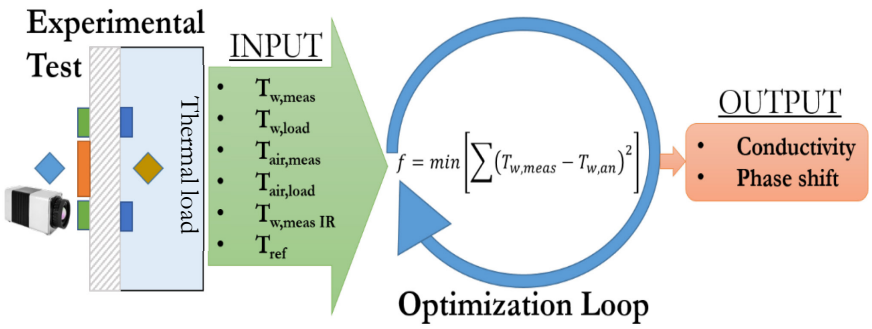

Figure 21. Soft-Sensing approach

3.1 Thermal contact sensors

3.1.1 Methodology

The method is based on the equation shown and described in the section 2.1 but with the difference that the thermal parameters (conductivity, density and specific heat) are the variables modified within the optimization tool in order to minimize the objective function $\Sigma(Tw,meas-Tw,an)^2$.

The optimization is implemented in MATLAB in the *fmincon* function, which allows identifying a local minimum value of the objective function in a specific range. At the range minimum value, the thermal properties of the component are set equal to the ones of the air (the lowest values of thermal conductivity and phase shift) and at the range maximum value the properties of the component are set equal to the ones of the concrete (i.e. material with a great heat capacity). It is clear that a small range would give a fast solution, but it requires a previous knowledge of the properties of the material under test. Nevertheless, in order to keep the optimization problem as blind as possible the variability range has been set with the farthest extrema.

The output of the model is the thermal conductivity of the panel under test, which gives, after several optimization loops the best fit between calculated and measured data.

3.1.2 Experimental Test

The measured data to be coupled with the calculated ones have been obtained from a testing campaigned focused on the thermal behavior characterization of two building component simulacra: a single layer Extruded Polystyrene (XPS) panel (called SL for Single Layer), the one described in section 2.2, and a double layer EPS (Expanded Polystyrene)-XPS panel (called DL for Double Layer).

In Table 6 the geometrical, thermal and mechanical properties of the two components are reported.

Table 6. Characteristics of the tested panels.

Panel	Material	Thickness [m]	k [W m^{-1} K^{-1}]	ρ [kg m^{-3}]	c_p [J kg^{-1} K^{-1}]
SL	XPS	0.03	0.032	30	1450
DL	XPS + EPS	0.03	0.034	20	1475

The thermal load has been imposed by using the same conditions described in the section 2.3 with a climatic room on one side of the panel under test, for both the panel. In this section the optimization will be based on the temperature measured on the response side of the panels by the thermocouples.

3.1.3 Results

– *Single Layer panel (SL)*

In Figure 22 the experimental temperature profile measured by the thermocouple is compared with the one calculated by the Soft-Sensing method at the end of the optimization loop. Their correlation is reported in Figure 23 that evidences a good correlation with a coefficient of determination of 0.99306.

This result is related to the thermal conductivity and the phase shift evaluated with the Soft-Sensing approach, respectively 0.032 W m^{-1} K^{-1} and 375 s, that accurately matches the thermal conductivity and the phase shift values declared by the producer of this panel, respectively 0.032 W m^{-1} K^{-1} and 385 s. In Table 7 the output of the Soft-Sensing method compared with the expected values are shown.

Table 7. Results and comparison with the certified values.

Panel	Thickness [m]	Certified Values		Soft-Sensing Results		*Discrepancy (δ)*
		Conductivity [W m^{-1} K^{-1}]	Phase [s]	Conductivity [W m^{-1} K^{-1}]	Phase [s]	*Conductivity [%]*
SL	0.03	0.032	385	0.032	375	*0*

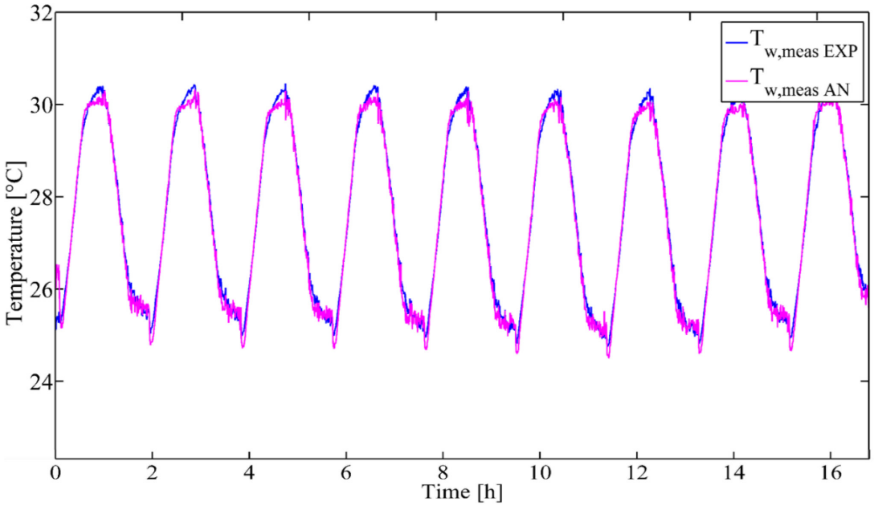

Figure 22. Temperature comparison between experimental and Soft-Sensing data

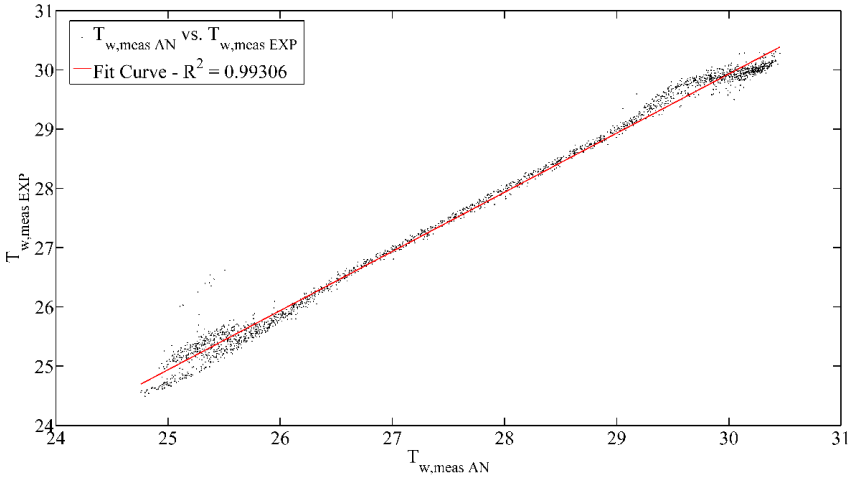

Figure 23. Correlation between experimental and Soft-Sensing data

– *Double Layer panel (DL)*

The same approach has been used on a sandwich panel made of two layers of Expanded Polystyrene and Extruded Polystyrene.

Each layer has a thickness of 0.03m. The properties of the sandwich panel, shown in Table 6, have been evaluated as equivalent value from the values of each layer, in accordance with Equation (20), based on electrical analogy of series of resistances.

$$R_{tot} = \sum_i R_i = \sum_i \frac{d_i}{k_i} \left[\frac{m^2 K}{W} \right] \tag{20}$$

where R_{tot} is teh total resistance, d_i the thickness of each layer, k_i the conductivity of each layer.

The same approach reported for the SL panel for the evaluation of the total density and specific heat of the sandwich panel has been used, obtaining the results shown in Table 8.

The experimental test has been done using the same conditions of the SL panel test. In this case the phase shift is almost 3 times the phase of SL panel but a time step of 1800s for the thermal load is sufficient to have good results with the Soft-Sensing method. In Figure 24 the temperature and heat flow profiles measured in the testing campaign are shown.

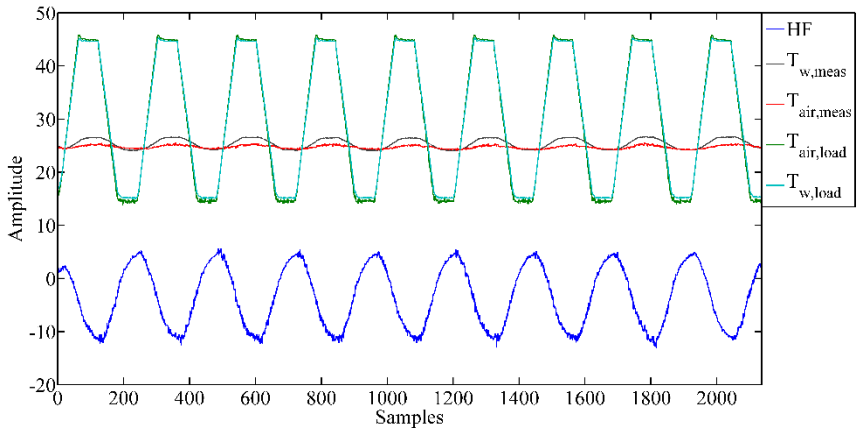

Figure 24. Temperature at both side of the Dl panel and heat flow profiles

Table 8. Results and comparison with the expected values.

Panel	Thickness [m]	Expected Values Conductivity [W m^{-1} K^{-1}]	Phase [s]	Soft-Sensing Results Conductivity [W m^{-1} K^{-1}]	Phase [s]	***Discrepancy (δ) Conductivity [%]***
DL	0.03	0.034	999	0.033	915	***2.9***

The results presented in the Table 8 show a conductivity value of 0.033 W m^{-1} K^{-1} against the expected conductivity value 0.034 W m^{-1} K^{-1} with a deviation of 2.9 %. The phase shift presents a result less accurate (915s against the expected value of 999s).

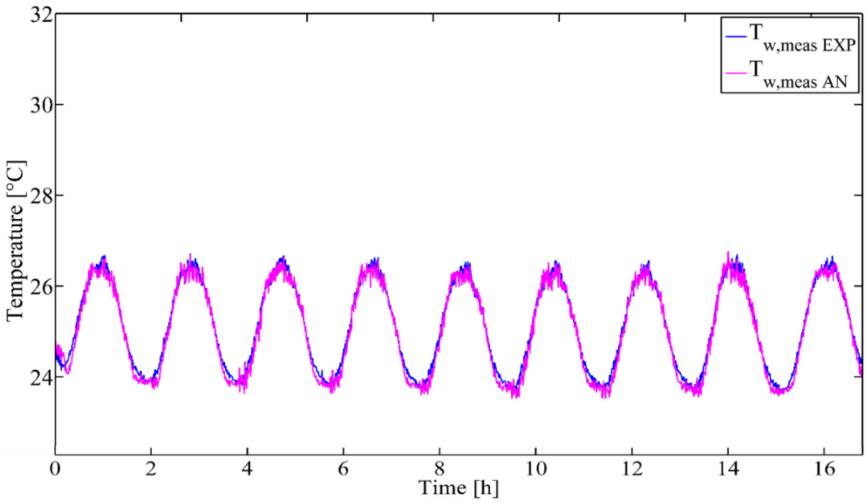

Figure 25. Temperature comparison between experimental and Soft-Sensing data

Figure 25 shows the surface temperature profiles obtained from the experiment (blue curve) and the ones calculated by the Soft-Sensing method.

The figure is presented with the same scale in amplitude of the temperature profile obtained for the SL panel, Figure 22, in order to make clearly visible the reduction in temperature at response side due to the increment of the thickness of the sandwich panel with respect to the SL panel.

The temperature profile obtained from the Soft-Sensing method matches the profile measured during the experimental test, with a determination factor, R^2, of 0.985, as shown in Figure 26.

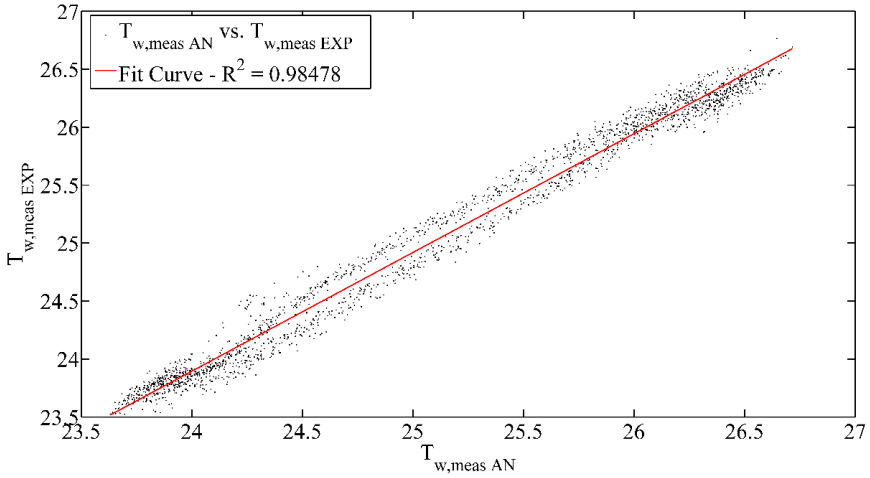

Figure 26. Correlation between experimental and Soft-Sensing data

3.2 IR sensor

3.2.1 Methodology

The Soft-Sensing methodology presented and validated in section 3.1 for temperature contact sensors has been applied to experimental data obtained by IR sensor (thermal camera).

The exploitation of a thermal camera allows having several advantages among which:

- The non-contact nature of the sensor shortening the set-up phase and allowing measurement on surface difficult to access as building envelope;
- The full-field visualization of the temperature distribution across the field of view of the camera, it allowing localizing eventual component discontinuities as thermal bridges.

On the other hand, the thermal camera has the disadvantage of being more sensitive to environmental conditions and external radiation with respect to a thermal contact sensor. For this reason, there is the necessity of monitoring the temperature reflected by the external environment on the observed object. The surface temperature of the component under test is evaluated in accordance with Equation (19) by imposing an air transmission coefficient (τ) of 0.99 and a panel surface emissivity (ε) of 0.97.

The emissivity of the panel surface is assessed in the calibration phase of the thermal camera, by comparing the thermal camera reading at a specific pixel with the temperature measured on the same pixel by a thermocouple.

Figure 27 shows the temperature profiles measured during the experimental test on the DL panel. In the figure, it is visible that the temperature measured at one pixel by the thermal camera matches the one measured by the thermocouple located at the same pixel after the correction of emissivity. The black curve represents the reflected temperature evaluated on an aluminum sheet positioned on the panel (low emissivity material).

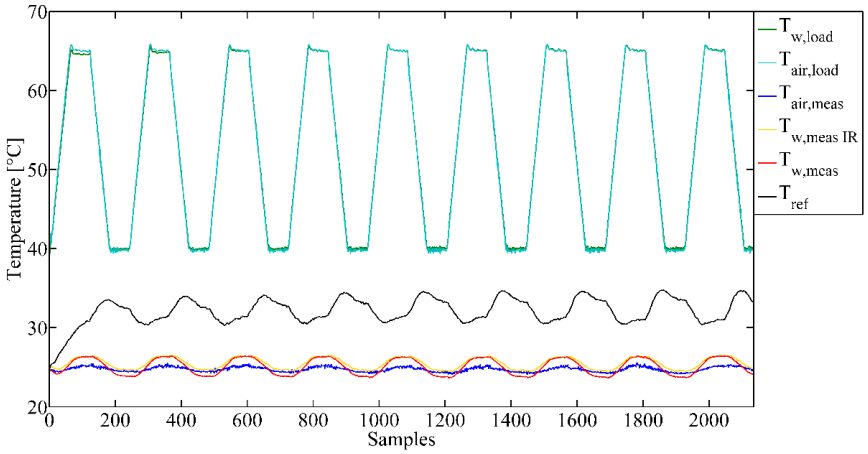

Figure 27. Experimental test data on DL panel

The test campaign has been done on the DL panel, using the same conditions described in section 3.1.2 but imposing a higher temperature in the load side; as shown in Figure 27, the range was set from 40 °C to 65 °C, in order to have a positive flow across the panel during the complete test duration.

3.2.2 Results

The thermal properties of the measured object are the same as the ones evaluated for thermal contact sensor as shown in the Table 6.

Table 9 shows the results obtained with the Soft-Sensing method applied to the IR sensor compared with the expected values.

Table 9. Results and comparison with the expected values.

Panel	Thickness [m]	Expected Values Conductivity [W m^{-1} K^{-1}]	Phase [s]	Soft-Sensing Results Conductivity [W m^{-1} K^{-1}]	Phase [s]	*Discrepancy (δ) Conductivity [%]*
DL	0.03	0.034	999	0.033	800	*2.9*

The results presented in Table 9 show a conductivity value of 0.033 W m^{-1} K^{-1} against the expected conductivity value 0.034 W m^{-1} K^{-1} with a deviation of 2.9 %. The phase shift presents a result less accurate (800s against the expected value of 999s).

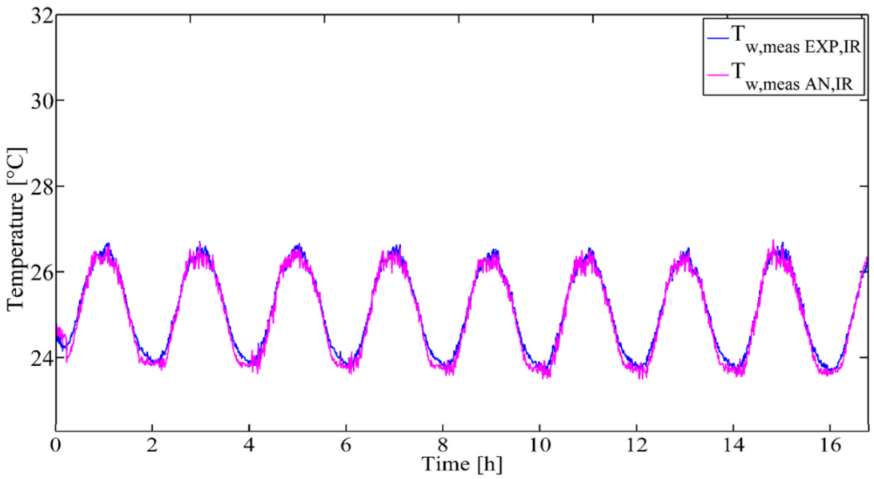

Figure 28. Temperature comparison between experimental and Soft-Sensing data

The Figure 28 shows the surface temperature profiles obtained from the experimental test (blue curve) and from the Soft-Sensing method.

The temperature profile obtained from the Soft-Sensing method matches perfectly the profile measured during the experimental test, with a determination factor, R^2, of 0.985, as shown in the Figure 29.

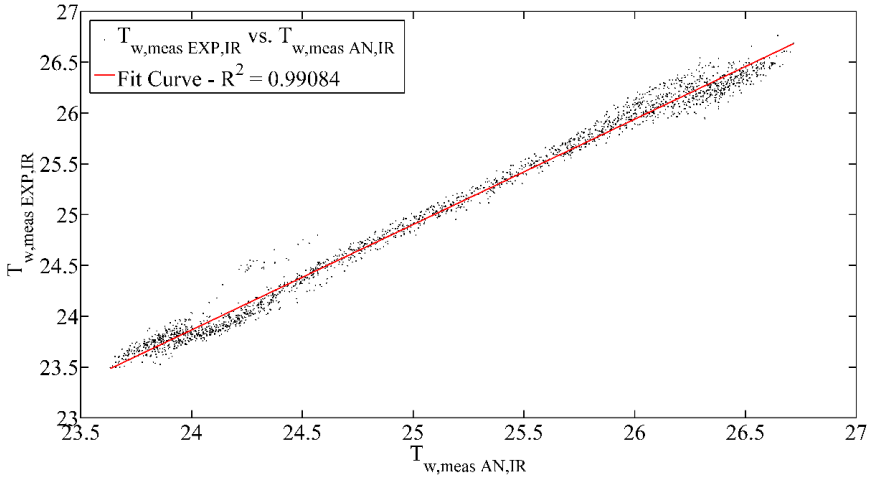

Figure 29. Correlation between experimental and Soft-Sensing data

3.3 Thermal transmittance estimation: comparison with standard methods

The output data of the Soft-Sensing method are the thermal and mechanical properties of the panel under test, from which the thermal transmittance can be derived. The real thermal conductance (C) and transmittance (U) of the panel can be calculated in accordance to the standards EN ISO 8990 [5] (laboratory test) and ISO 9869-1 [6] (in-situ test) by using Equation (21) and Equation (22) respectively:

$$C = \frac{\sum_{j=1}^{n} q_j}{\sum_{j=1}^{n} \left(T_{sij} - T_{sej} \right)} \left[\frac{W}{m^2 K} \right] \tag{21}$$

where q is the heat flow across the component, T_{si} the internal surface temperature and T_{se} the external surface temperature.

$$U = \frac{\sum_{j=1}^{n} q_j}{\sum_{j=1}^{n} \left(T_{ij} - T_{ej} \right)} \left[\frac{W}{m^2 K} \right] \tag{22}$$

where T_{si} is the internal environmental temperature and T_{se} is the external environmental temperature.

The summations in the Equation (21) and the Equation (22) are used only in in-situ test in order to mediate the acquired data to remove random errors, like external light radiation, until a convergence to an asymptotical value is observed.

In the laboratory test, the evaluation must be done in a steady-state condition, considering instantaneous values of flow and temperatures.

The difference between conductance, Equation (21), and transmittance, Equation (22), is related to the air resistances in both sides of the component that are not considered in the evaluation of the thermal conductance.

Equations (21) and (22) are valid for surface wall temperatures measured by contact sensors. In the case of the surface temperature is measured by a thermal camera the air resistance is included in the temperature to which the sensor is sensitive. Therefore, the thermal transmittance cannot be estimated from the conductance but by applying a direct method, which is based on the energy balance at the boundary of the observed component [3]. This method exploits Equations from (1) to (4) by substituting Equation (2) with Equation (23) in order to introduce the thermal transmittance in the relation:

$$\dot{Q} = UA\left(T_{air,meas} - T_{air,load}\right)\left[\frac{W}{m^2}\right] \tag{23}$$

By combining Equation (23) and Equation (1) the thermal transmittance can be written as Equation (24):

$$U = \frac{4\sigma\varepsilon T_{w,meas}^3\left(T_{w,meas} - T_{ref}\right) + h_c\left(T_{w,meas} - T_{air,meas}\right)}{T_{air,meas} - T_{air,load}} \tag{24}$$

The standards EN ISO 8990 and ISO 9869-1 [6] states that the thermal transmittance calculated in their accordance has an uncertainty less than 8 %. The thermal transmittance evaluated by thermal camera and by means of Equation (24) has an uncertainty in the range of 10-20 % [3].

The tests have been made on the SL panel, by using the same setup shown in the Figure 13. For this panel the conductivity value obtained with the Soft-Sensing approach is 0.032 W m^{-1} K^{-1} that corresponds to a thermal transmittance value, *U*, of 0.903 W m^{-2} K^{-1} and to a thermal conductance value, *C*, of 1.067 W m^{-2} K^{-1}.

Two different tests have been conducted with different thermal loads:

– Steady-state test: with a fixed temperature value in the load side in order to reproduce the laboratory test described by the standard EN ISO 8990. The data acquired are shown in Figure 30.

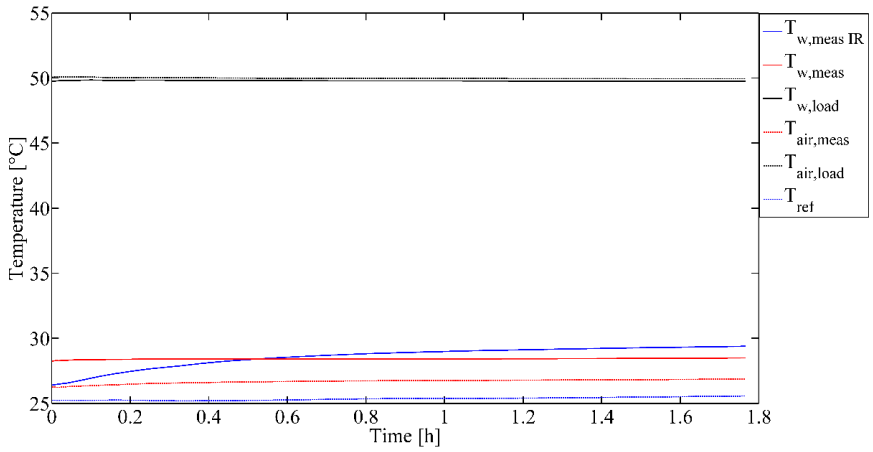

Figure 30. Temperature profiles acquired during the stationary test

– Time varying test: the same experimental test described in the section 3.2.1 in order to reproduce the in-situ test described by the standard ISO 9869-1. In Figure 27 the data acquired are shown.

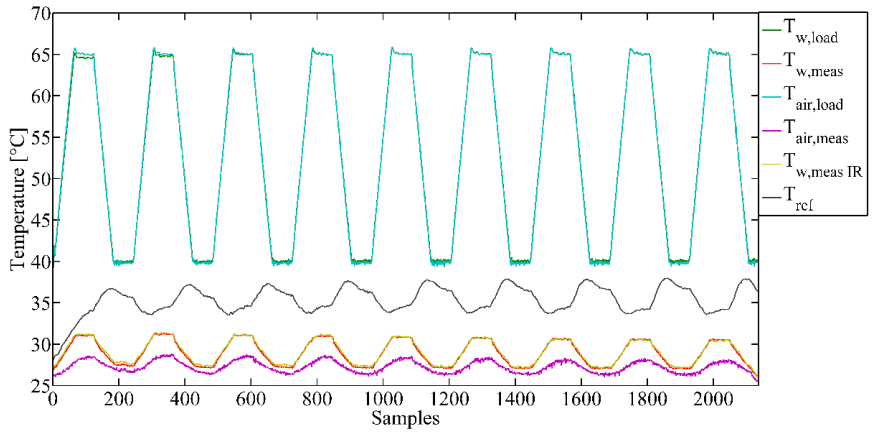

Figure 31. Temperature profiles acquired during the stationary test

3.3.1 Results

– *Stationary Test (EN ISO 8990)*

The standard EN ISO 8990 [5] defines the steady-state condition with a discrepancy between temperatures and flows acquired in different instants of the test less than 1 % and imposes a difference of temperature between the opposite sides of the component at least of 20 °C.

In Figure 32 the thermal conductance obtained during all the test is shown, while in Figure 33 the thermal transmittance evaluated is shown.

The final value obtained at the end of the test is 1.111 W m^{-2} K^{-1} of thermal conductance and 0.908 W m^{-2} K^{-1} of thermal transmittance obtained with the heat flux transducer while with the IR sensor the values obtained are respectively 1.326 W m^{-2} K^{-1} and 1.046 W m^{-2} K^{-1}.

Table 10. Results and comparison with the certified values and stationary test.

Values [W m^{-2} K^{-1}]			*Discrepancy (δ) [%]*
Certified Values	*Conductance*	*1.067*	-
	Transmittance	*0.903*	-
Heat Flux Transducer [5]	Conductance	1.111	*4.2*
	Transmittance	0.908	*3.4*
IR sensor method [3]	Conductance	1.326	*24.3*
	Transmittance	1.046	*19.2*
Soft-Sensing method	Conductance	1.067	*0*
	Transmittance	0.903	*0*

In Table 10 the results of the stationary test with both the standard methods (heat flux transducer and IR sensor) compared with the expected values and the ones obtained with the Soft-Sensing approach are shown. The discrepancies in the results are in line with the values found in the literature that establish an error smaller than 8% for the heat flux transducer method and around the 20% for the IR sensor method.

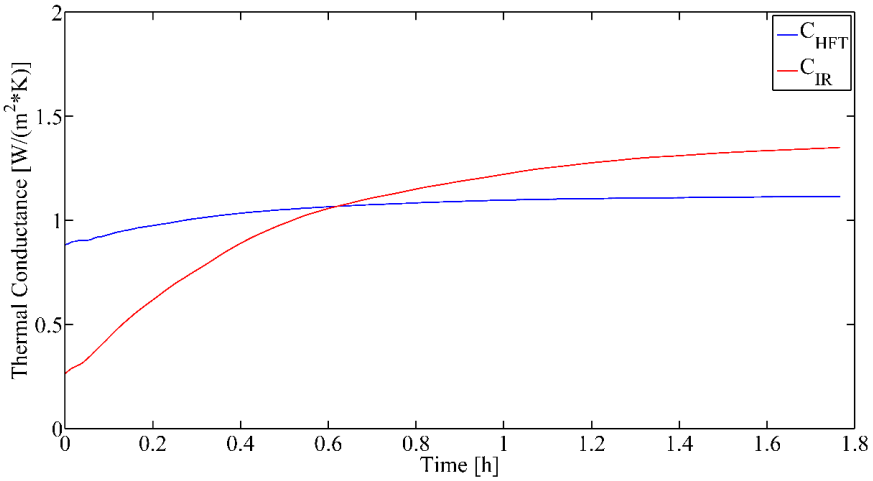

Figure 32. Thermal conductance evaluated during the stationary test

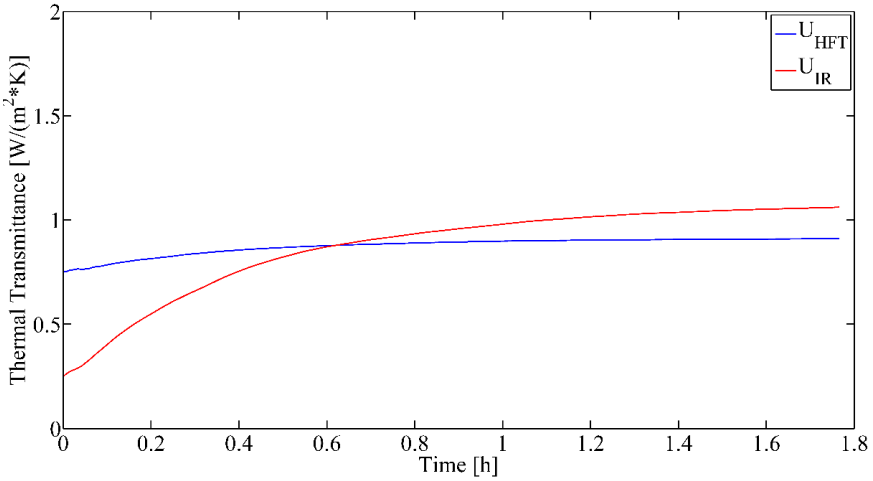

Figure 33. Thermal transmittance evaluated during the stationary test

– *In-situ Test (ISO 9869-1)*

The standard ISO 9869-1 [6] defines the in-situ test with natural thermal load on one side of the building component observed. It means that a cyclic load (night/day)

is considered. The standard establishes that the test duration must be at least of 72h if the temperature is stable otherwise, this duration may be more than 7 days.

It is recommended that the analysis is carried out only on data acquired at night to avoid the effects of the solar radiation on the external surface. The test could be stopped when the results after three subsequent nights do not differ by more than ±5%.

The analysis must be done by applying a progressive average on the acquired data in accordance with the Equation (21) and the Equation (22) in order to reduce random phenomena effects on the evaluation.

The experimental test has been done by simulating the in-situ conditions and after the application of the progressive average, the data shown in Figure 31 becomes as reported in Figure 34.

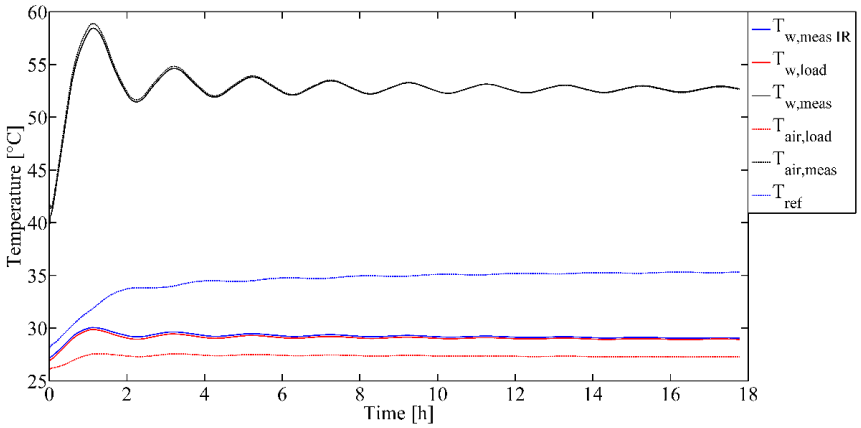

Figure 34. Temperature profiles processed with the progressive average

In Table 11 the results of the time varying test compared with the expected values and the obtained one with the Soft-Sensing approach are shown.

Table 11. Results and comparison with the certified values and time-varying test.

Values [W m^{-2} K^{-1}]			*Discrepancy (δ) [%]*
Certified Values	***Conductance***	***1.067***	-
	Transmittance	***0.903***	-
Heat Flux Transducer [6]	Conductance	1.185	***11.1***
	Transmittance	0.956	***8.9***

IR sensor method [3]	Conductance	1.481	*38.9*
	Transmittance	1.140	*29.9*
Soft-Sensing method	Conductance	1.067	*0*
	Transmittance	0.903	*0*

The final value obtained at the end of the test is 1.185 W m^{-2} K^{-1} of thermal conductance and 0.956 W m^{-2} K^{-1} of thermal transmittance obtained with the heat flux transducer while with the IR sensor the values obtained are respectively 1.481 W m^{-2} K^{-1} and 1.140 W m^{-2} K^{-1}.

Also in this case the discrepancies in the results are in line with the values found in the literature (8% for the heat flux transducer method and 20% for the IR sensor method) but are greater than the obtained one with the stationary test.

In Figure 35 the thermal conductance obtained during all the test is shown, while in the Figure 36 the thermal transmittance evaluated is shown.

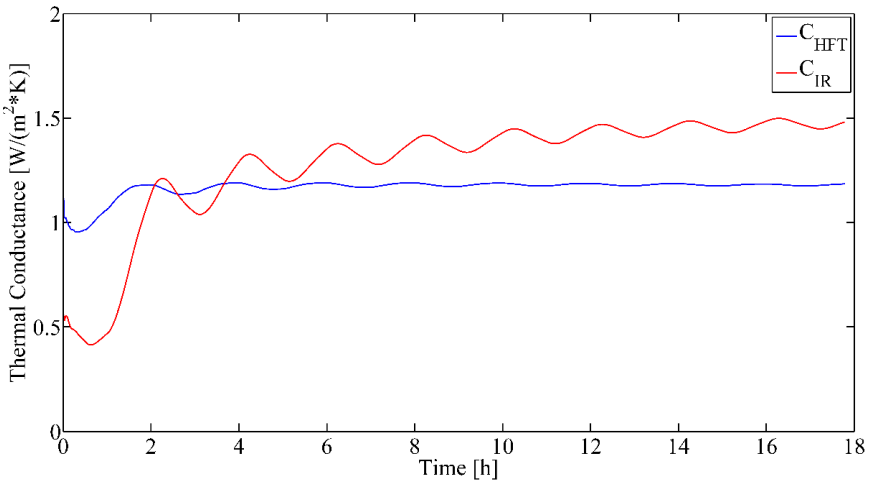

Figure 35. Thermal conductance evaluated during the time-varying test

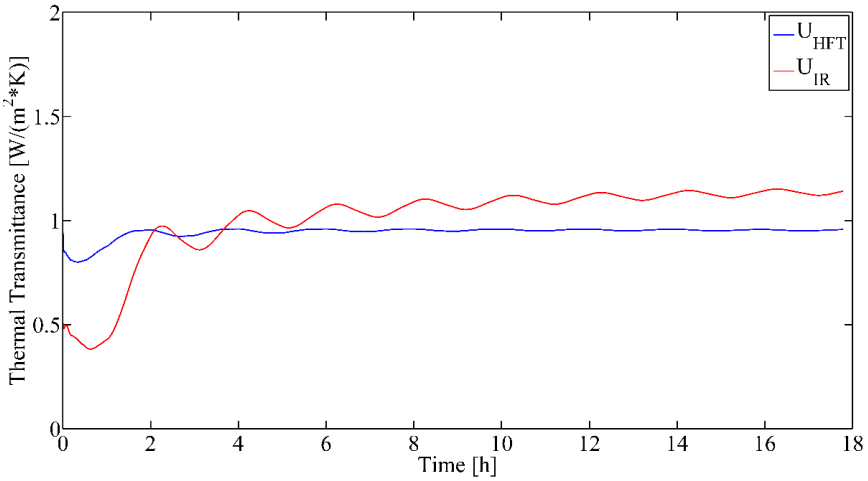

Figure 36. Thermal transmittance evaluated during the time-varying test

Chapter 4

Uncertainty & sensitivity analysis

4.1 Uncertainty analysis

When reporting the result of a measurement of a physical quantity, it is mandatory that some quantitative indication of the quality of the result be given so that those who use it can assess its reliability. [22]

In order to assess the uncertainty of the Soft-Sensing method described in section 3 two complementary studies have been conducted:

- Analytical uncertainty determination of the surface emissivity by applying the combined standard uncertainty method
- Soft-Sensing method uncertainty estimation by means of a Monte Carlo by considering the uncertainties of the sensors applied and the emissivity uncertainty evaluated in the previous step.

4.1.1 Emissivity uncertainty estimation

The GUM [22] defines the combined standard uncertainty, $u_c(y)$, as the positive square root of the combined variance, $u_c^2(y)$, which is given by Equation (25).

$$u_c^2(y) = \sum_{i=1}^{N} \left(\frac{\partial f}{\partial x_i} \right)^2 u^2(x_i) \tag{25}$$

where f is the analytical function representing the relation between the dependent variable (y) and the independents ones (x_i).

The analytical formulation for the emissivity evaluation of the material is Equation (26).

$$\varepsilon = \frac{T_{cam}^4 - \tau T_{ref}^4 - (\tau - \tau^2) T_{air,meas}^4}{T_{w,meas}^4 - T_{ref}^4} = \frac{T_{cam}^4 - T_{ref}^4}{T_{w,meas}^4 - T_{ref}^4} \tag{26}$$

where the right hand-side of the Equation (26) is obtained by considering the environmental transmissivity, τ, equal to 1.

The variables in the previous equation are the temperatures measured by thermocouples and thermal camera and their uncertainty has been taken from the manufacturer's specification:

- Thermocouples: ± 0.5 °C, ±2σ, this is the uncertainty associated to Tref and Tw,meas
- Thermal camera: ± 1.5 °C, ±2σ, this is the uncertainty associated to Tcam.

Equation (25) written for the material emissivity becomes:

$$u_c^2(\varepsilon) = \left(\frac{\partial f}{\partial T_{cam}}\right)^2 u^2(T_{cam}) + \left(\frac{\partial f}{\partial T_{ref}}\right)^2 u^2(T_{ref}) + \\ + \left(\frac{\partial f}{\partial T_{w,meas}}\right)^2 u^2(T_{w,meas}) \tag{27}$$

From Equation (27) the uncertainty associated to the emissivity $u_c(\varepsilon)$ is ±5.5%.

4.1.2 Thermal transmittance uncertainty estimation

The GUM defines the uncertainty assessment of a numerical model by using a Monte Carlo method.

This approach is based on the generation of uniform distribution of data associated to each sensor uncertainty used as input for the model, in order to have a statistical distribution of the population from which is possible to evaluate the uncertainty of the model in terms of standard deviation [23].

In order to deliver a 95 % coverage interval for the output quantity a number of 10^6 trials for each variable in the model is required.

For each measured data used in the evaluation, the uncertainty of the specific sensor has been used, as shown in the Table 12, and the Monte Carlo simulation has been done by generating random numbers in these uncertainty ranges by assuming a uniform distribution. For each variable a matrix *m*n* number of elements has been generated, where *m* represents the number of samples acquired for each variable (63000 samples in the data tested with the Monte Carlo simulation acquired with a sampling time of 1s) and *n* is a custom number defined in order to have at least 10^6 iterations (16 in this evaluation).

Table 12. Uncertainties of the measured quantities.

Measured quantity	Sensor	Evaluation*	$u(x_i)$
$T_{w,load}$	Thermocouples	Datasheet	± 0.5 °C
$T_{w,meas}$	Thermal Camera	Datasheet	± 1.5 °C
$T_{air,meas}$	Thermocouple	Datasheet	± 0.5 °C
ε	Thermocouples/Thermal camera	Analytical (section 4.1.1)	± 5.5 %
Air velocity, v	Anemometer	Datasheet	± 4 %

*uncertainty values from the sensor's datasheets except for the emissivity that has been calculated as described in section 4.1.

The distribution of the thermal conductivity of the panel under test, obtained by running the Soft-Sensing model with the 10^6 trials simulated by the Monte Carlo method is shown in Figure 38. It is clear that the distribution is Gaussian and can be fitted with a normal probability distribution function (the red line in Figure 37). The mean value of the distribution is 0.0321 W m^{-1} K^{-1} 0.0321 W m^{-1} K^{-1} that matches the expected conductivity (0.032 W m^{-1} K^{-1}).

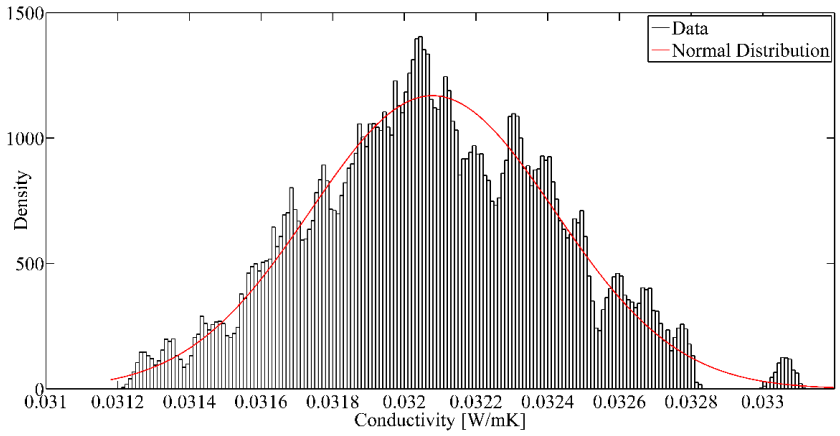

Figure 37. Thermal conductivity distribution estimated with the Monte Carlo simulation

The standard deviation of the conductivity distribution is 0.362*10^-3 W m^{-1} K^{-1}. The conductivity percentage relative uncertainty estimated by considering a coverage is ±3.4 %. This value is less than the declared uncertainty value for the standard test

found in the literature (8 % for the heat flux transducer method [24] and 20 % for the IR sensor method [3]).

The result obtained from the Monte Carlo simulation represents the uncertainty related to the accuracy of the sensors and of the measurement chain. Other aspects should be taken into account for a better evaluation, like the fluctuation of environmental conditions and the discrepancy between the model and the object under test but at this stage their contributions are very difficult to quantify.

4.2 Sensitivity analysis

In order to understand the effective applicability of the proposed approach in real environmental conditions, a sensitivity analysis of the method to influencing parameters has been performed.

Specifically, an experimental test campaign has been conducted in order to estimate the influence of the following parameters on building element transmittance evaluation:

- Air velocity, which has been varied by means of a fan and measured with an anemometer.
- Material emissivity, whose variation has been reproduced by painting the observed area with different emissivity paints.
- External radiation that has been realized by using an IR lamp mounted behind the thermal camera.

The sensitivity analysis has been done first considering the influence of each parameter varied independently and afterwards they have been changed simultaneously, in order to reproduce the most unfavorable condition.

Finally, in order to underline the advantages given by the Soft-Sensing approach in terms of test duration and uncertainty reduction, an evaluation of the results in function of the number of cycle of the thermal load has been conducted.

4.2.1 Experimental setup

The experimental setup used for the test campaign is the same already shown in the section 2.3 with in addition a fan, a IR lamp, an anemometer and a thermal microclimate data logger to acquire the data from the anemometer.
In Table 13 the anemometer and the data logger used for the experimental test and their specifications are shown.

Table 13. Sensors' datasheets.

Tool Type	Model	Specifications
Anemometer	Delta OHM – AP3203	Sensor type: NTC 10kOhm Measurement Range: 0 to 80 °C Measurement Range: 0.05 to 5 m s^{-1} Accuracy: ±0.02 m s^{-1} (< 1 m s^{-1}) Accuracy: ±0.1 m s^{-1} (< 5 m s^{-1})
Thermal microclimate data logger	Delta OHM – HD32.1	Channels: 8 Operative Conditions: -5 to 50 °C

In Figure 38 the microclimate station is shown.

Figure 38. Microclimate station

In Figure 39 the experimental setup is shown.

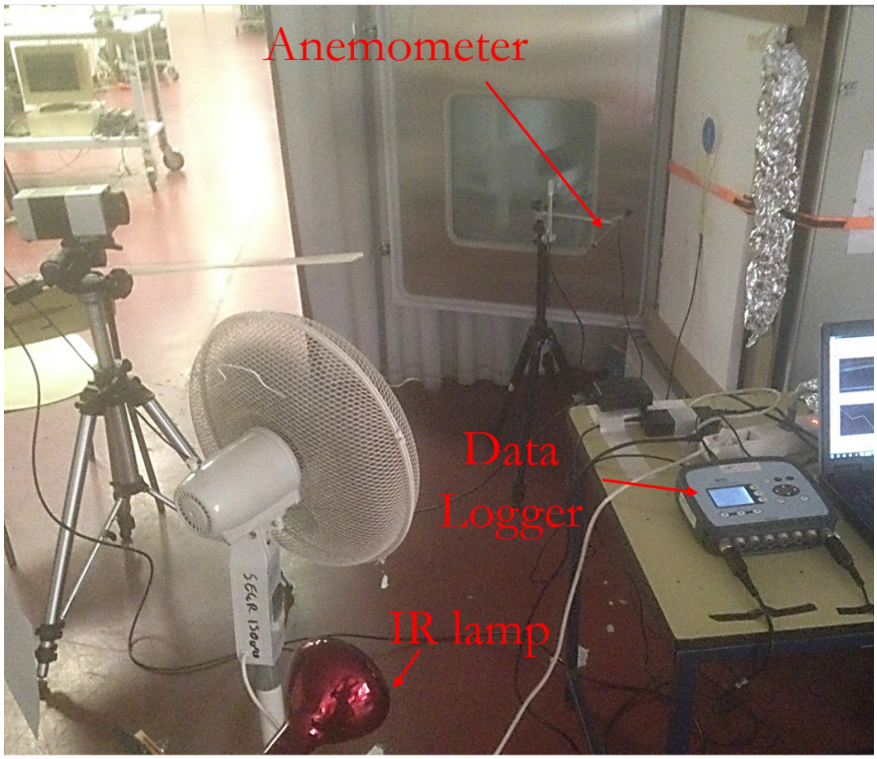

Figure 39. Measurement setup

The test campaign has been conducted on a different panel in respect to the ones shown in the section 3.1.2, but with similar thermal properties. This panel, called E-SL, is a single layer EPS panel with a thermal conductivity k = 0.0374 W m^{-1} K^{-1}.

In the Table 14 the thermal properties of the tested panel are shown.

Table 14. Characteristics of the tested panel.

Panel	Material	Thickness [m]	k [W m^{-1} K^{-1}]	ρ [kg m^{-3}]	c_p [J kg^{-1} K^{-1}]
E-SL	EPS	0.03	0.0374	15	1450

4.2.2 Air velocity

The analysis has been conducted by generating different air velocity fields in the external side of the panel in order to reproduce different ambient conditions in term of wind that can occur in real measurements performed outside. According to the Beaufort wind force scale standard, [25], three levels of velocity have been reproduced:

- 0.5 m s^{-1} (calm)
- 1 m s^{-1} (light air)
- 2 m s^{-1} (light breeze)

The air velocity has been monitored during the test by means of an anemometer.

The tests have been conducted by imposing a cyclic load between 30 and 50°C in the climatic room.

In Figure 40 an example of the acquired data, during the test with 2 m s^{-1} air velocity, is shown.

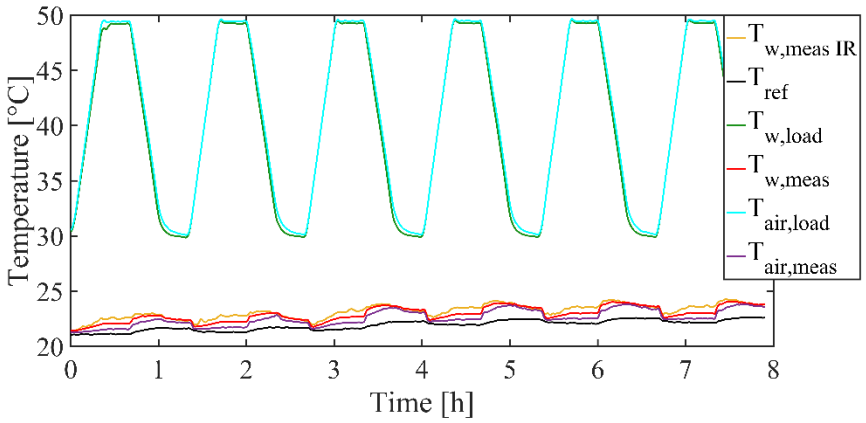

Figure 40. Temperature profiles during the test with 2 m s^{-1} air velocity

The comparison has been done between standard method (heat flow method defined by the standard ISO 9869-1) and both the Soft-Sensing approaches (with contact sensors and with IR sensor). The thermal conductivities measured with the different methodologies for all the tests with different air velocity show a variability less than the typical uncertainty of the standard measurement technique, heat flow transducer method, i.e. ±5%, see Table 15. This result shows how the methodologies

are not sensitive to the air velocity changes in the velocity range considered (from 0.5 to 2 m s^{-1}). For this reason, we can assume the same thermal conductivity value for each air velocity considered during the tests. In Table 15 the results obtained and the mean values used for each method for all the velocities are shown.

Table 15. Results of the experimental tests with different air velocity.

v [m s^{-1}]	**Thermal conductivity [W m^{-1} K^{-1}]**		
	ISO 9869-1	Soft-Sensing (HF)	Soft-Sensing (IR)
0.5	0.0379	0.0379	0.0375
1	0.0369	0.0368	0.0372
2	0.0385	0.0377	0.0376
μ	**0.0378**	**0.0375**	**0.0374**
2σ	**±1.1e^{-3} (±2.9%)**	**±6.3e^{-4} (±1.7%)**	**±2.7e^{-4} (±0.7%)**
Expected Value 0.0374 ±5.0% [W m-1 K-1]			

As already shown in the section 2.1 the thermal transmittance value depends by the surface resistance, R_s. in accordance with the Equations (6), (7) and (10) the surface resistance values (load and measured sides) depends by the air velocity and external radiation. During the tests with different air velocity, the surface resistance on the load side is the same (0.064 m^2 K W^{-1}) while in the measured side it decreases when the air velocity increases (0.084 m^2 K W^{-1} for air velocity of 0.5 m s^{-1}, 0.072 m^2 K W^{-1} for air velocity of 1 m s^{-1} and 0.056 m^2 K W^{-1} for air velocity of 2 m s^{-1}).

The thermal transmittance has been evaluated by using the mean thermal conductivity value obtained for each method (shown in the Table 15) but using the different surface resistances related to air velocity changes. For this reason, the expected thermal transmittance value changes in each test, as shown in the Table 16.

Table 16. Results of the experimental tests with different air velocity.

v [m s^{-1}]	Thermal transmittance [W m^{-2} K^{-1}]				Discrepancy (δ) from the expected value [%]		
	ISO 9869-1	Soft-Sensing (HF)	Soft-Sensing (IR)	**Expected value**	ISO 9869-1	Soft-Sensing (HF)	Soft-Sensing (IR)
0.5	1.062	1.0549	1.0525	**1.0525**	0.90	0.23	0
1	1.0757	1.0684	1.0659	**1.0659**	0.92	0.24	0
2	1.0945	1.087	1.0844	**1.0844**	0.93	0.24	0

The results show a low level of discrepancy between the expected value and the obtained one with all the methods compared (less than 1%).

4.2.3 Material emissivity

One of the most important aspects in the IR analysis is represented by the emissivity value of the observed material. This parameter influences the radiation emitted by the material and in consequence the temperature estimated by an IR sensor.

For this reason, an erroneous assessment of the material emissivity can decrease the accuracy of the Soft-Sensing method based on IR measurement data.

In order to understand the influence of this parameter on the assessment of the dynamic thermal behaviour of the material with the proposed method, an analysis has been conducted by painting the EPS panel with two different low emissivity paints. Table 17 reports the specifications of the paints used.

Table 17. Paints' specifications.

Paint	**Model**	**Emissivity**
Silver	Dupli Color	0.35
Chrome	Dupli Color	0.43

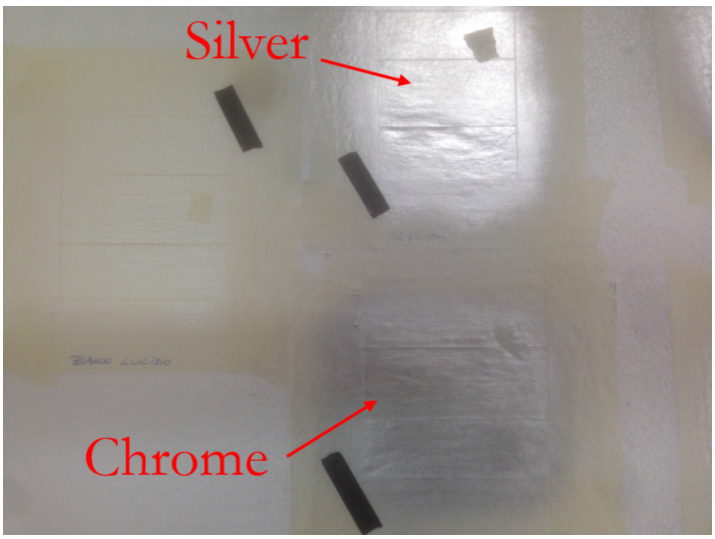

Figure 41. Painted panel

In Figure 41 the painted areas of the EPS panel tested are shown.

The tests have been conducted with 0.5 m s^{-1} air velocity in the measured side of the panel.

In Figure 40, the acquired data during the test is shown. The data called "RAW" represents the data acquired by the IR sensor without the emissivity correction. The black curve shows the temperature profile measured with a contact sensor (thermocouple).

Looking the image below it is clear that the temperature evaluation with the IR sensor is very close to the real temperature when the emissivity is near to 1 (see the red curve that represents the temperature profile of the EPS panel without paint).

When the emissivity decreases the discrepancy between the measured temperature value and the real one increases, see silver and blue dashed curves respectively for chrome and silver paints, and the emissivity correction is necessary.

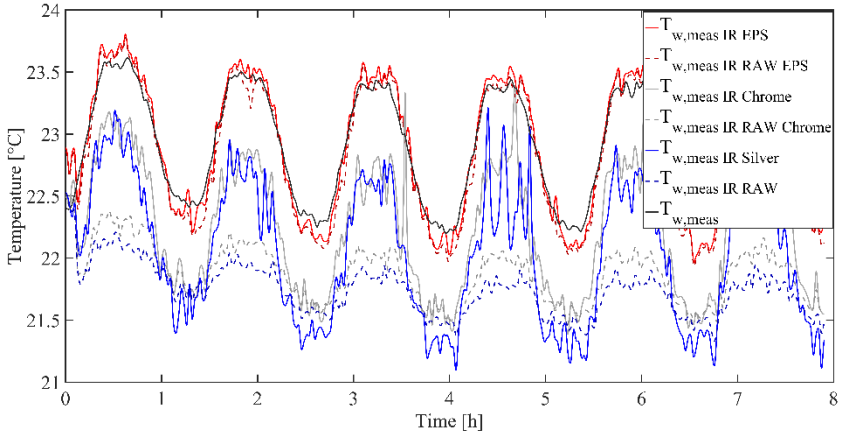

Figure 42. Temperature profiles during the test with 0.5 m s^{-1} air velocity

In the Table 18 the results for the different painted areas are shown.

Table 18. Results of the experimental tests on the painted areas.

Expected Thermal Transmittance = 1.0525 [W m^{-2} K^{-1}]

v [m s^{-1}]		Soft-Sensing (IR-EPS)	Soft-Sensing (IR-Silver)	Soft-Sensing (IR-Chrome)
0.5	Thermal Transmittance [W m^{-2} K^{-1}]	1.0525	1.0094	1.0238
	δ [%]	**0**	**4.1**	**2.73**

The results show how the discrepancy between the expected value of thermal transmittance and the obtained one increases up to 4% in the more complex case (low emissivity of the material). This value represents a border line value in terms of discrepancy considering the very low value of emissivity (≈ 0.3).

4.2.4 Radiative source

In order to understand the contribution of the emissivity and the external radiative source on the sensitivity of the methodologies, an IR lamp has been mounted behind the IR camera.

The lamp has been switch on periodically during the test, as shown by the reflected temperature profile in the Figure 43.

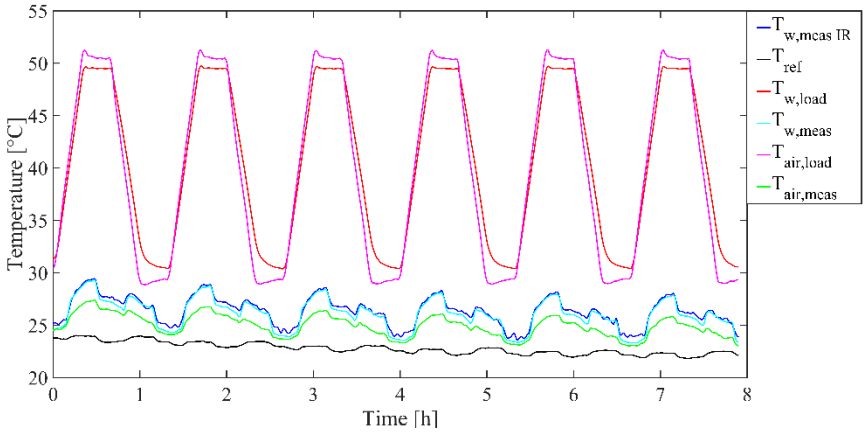

Figure 43. Temperature profiles during the test with IR lamp

In this test the fan has been switch off so for the thermal transmittance evaluation the surface resistance used is the ones proposed by the standards for indoor environmental conditions (0.13 m^2 K W^{-1}).

The results, reported in the Table 19, show how the external radiative source do not increase the uncertainty of the methodologies tested.

Table 19. Results of the experimental tests with IR lamp.

Expected Thermal Transmittance = 1.0039 [W m^{-2} K^{-1}]				
v [m s^{-1}]		ISO 9869-1	Soft-Sensing (HF)	Soft-Sensing (IR-EPS)
0	Thermal Transmittance [W m^{-2} K^{-1}]	1.0275	0.9865	0.9952
	δ [%]	**2.35**	**1.73**	**0.87**

4.2.5 Random perturbation

In order to have a more comprehensive evaluation of the method sensitivity a test has been conducted considering all the sources of influence described in the previous sections but combined in a random perturbation effect during the test.

- The air velocity has been varied during the test
- The IR lamp has been switch on during the test
- The panel under investigation was the one reported in the Figure 41, i.e. with different emissivity regions.

In Figure 44 the experimental setup is shown.

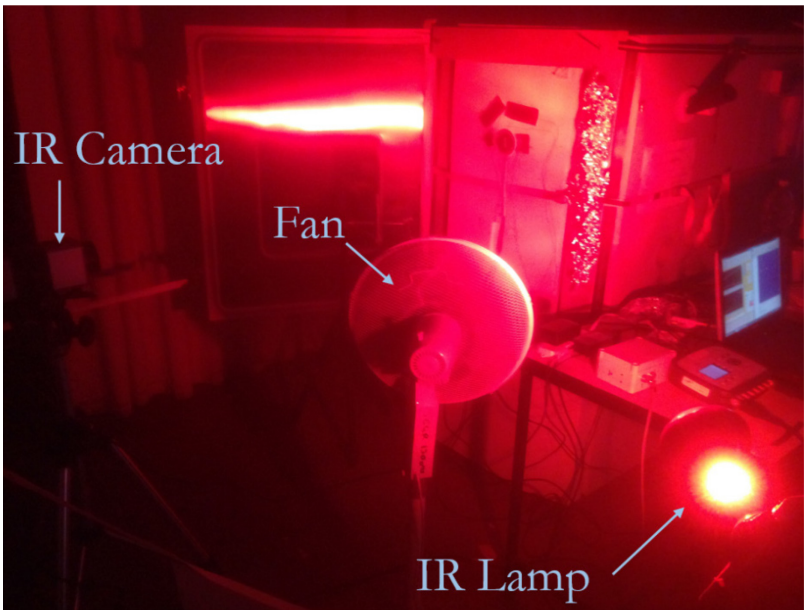

Figure 44. Experimental setup for random perturbation

In Figure 45 the load profile and both the air velocity profile and the IR source profile are shown. While in Figure 46 acquired data is shown.

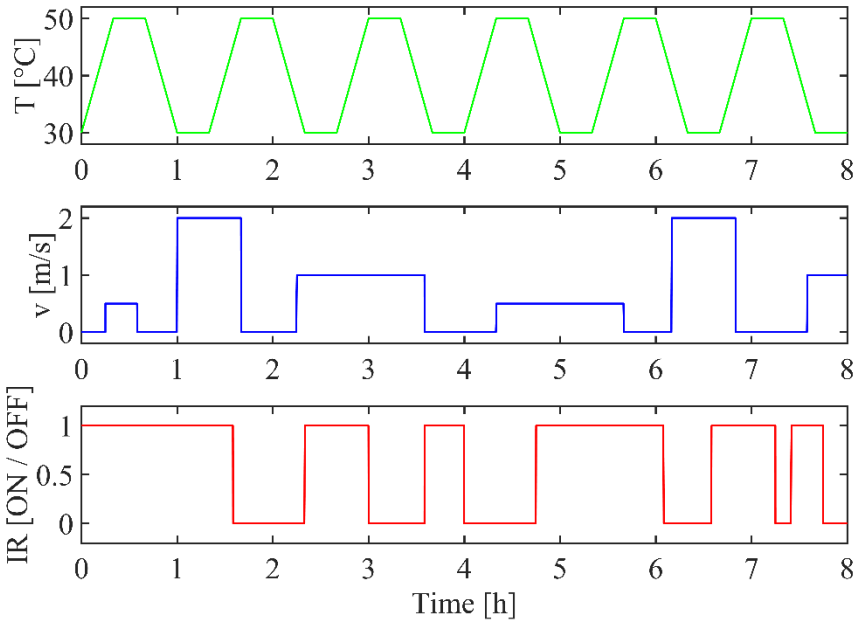

Figure 45. Time profiles of the thermal load, air velocity and IR lamp

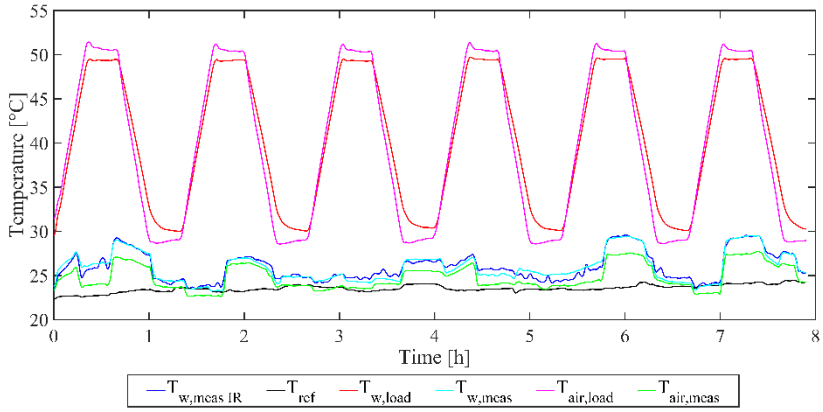

Figure 46. Temperature profiles during the test with random perturbation

The comparison has been done between standard method (heat flow method defined by the standard ISO 9869-1) and both the Soft-Sensing approaches (with contact sensors and with IR sensor) on the not painted area and with Soft-Sensing with IR sensor data on the painted areas.

The results are shown in terms of thermal conductance in Table 20, due to the fact that the air velocity changed during the test and so the surface resistance of the measured side of the panel changed during the test.

Table 20. Results of the experimental tests with random perturbation.

Expected Value C = 1.2567 [W m^{-2} K^{-1}]						
v [m s^{-1}]		ISO 9869-1	Soft-Sensing (HF)	Soft-Sensing (IR-EPS)	Soft-Sensing (IR-Silver)	Soft-Sensing (IR-Chrome)
0.5…2	C [W m^{-2} K^{-1}]	1.3567	1.2133	1.2233	1.1867	1.1933
	δ [%]	**7.96**	**3.45**	**2.66**	**5.57**	**5.05**

The experiments reported in this chapter show a situation completely different with respect to the results obtained in absence of disturbing sources. In fact, regarding the Soft-Sensing method the discrepancy between the expected thermal conductance and the obtained one is near to 3% both for the contact sensor approaches and for the IR sensor approach.

The same approach based on IR sensor data on the painted areas (low emissivity paints) shows a discrepancy up to 5% in the more unfavorable environmental conditions (variable air velocity and radiative external source). This value is less than the uncertainty value declared for the actual standard method (heat flow meter method), around 8%.

The uncertainty value of the standard method found in the literature fit well with the discrepancy value obtained following the standard ISO 9869-1 during the test campaign described in this section. In fact, a value up to 8% has been reached during the tests and this result shows how the heat flow meter method is more affected than the Soft-Sensing method by the environmental condition changes during the measurements.

The benefits of the Soft-Sensing method are more clear evaluating the final result in function of the number of load cycles, as shown in the Figure 47 (the dashed lines in the figure represents the ±5% limits defined by the standard for the thermal transmittance evaluation). The fluctuations of the profile obtained with the heat flow

meter show how the new proposed approach represents an enhancement in respect to the actual state-of-the-art in terms of time consuming and accuracy.

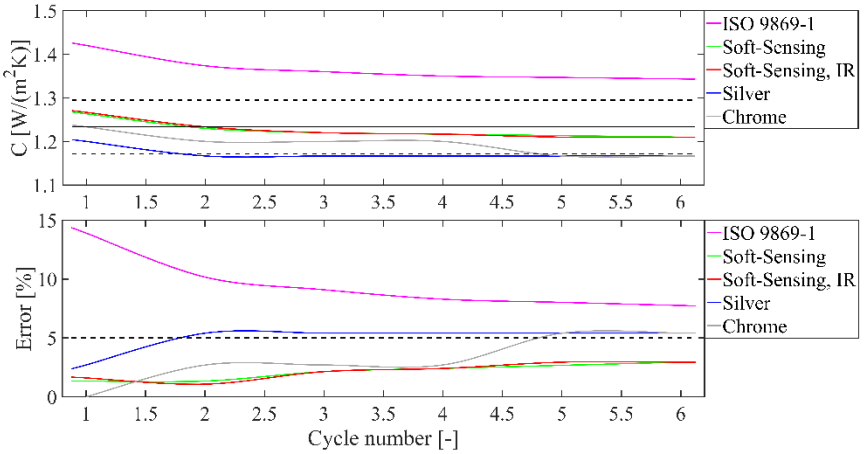

Figure 47. Results of different methods in respect to the number of load cycles

Chapter 5

Experimental proof of concept

A building room mock-up has been realized at the UNIVPM laboratory in order to validate the Soft-Sensing method proposed in a more complex case study.

The main advantage of the developed mock-up is its flexibility that allows replacing one of its walls with prefabricated panels realized ad hoc by DRAGADOS.

In the following sections the pilot testing mock-up and the experimental tests will be described.

5.1 Pilot test case

The pilot testing mock-up consists of a climatic room with the dimensions of 2230x2230x2030 mm^3, Figure 48.

Figure 48. Pilot testing mock-up

The room walls are sandwich panels of 100 mm thickness consisting of two external white pre-painted hot galvanized steel sheet layers filled with polyurethane.

In the Figure 49 the drawing of the room and the scheme of the main components (e.g. connections) are shown.

The left wall marked in red in the room's drawing can be dismantled and replaced with the prefabricated panel to be tested.

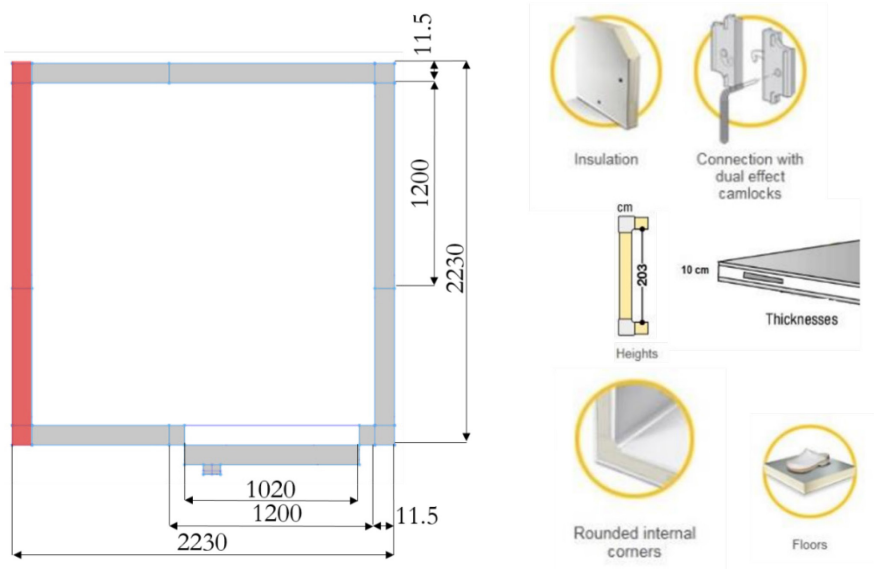

Figure 49. Drawing of the mock-up and components scheme

The prefabricated panel tested has been provided by DRAGADOS and presents an opening for a window and a pipe of 40 mm diameter inserted at mid-thickness.

The panel consists in a double layer of glass fiber reinforced concrete (GRC) and an insulating layer in expended polystyrene (EPS).

Furthermore, the panel presents an inner structure in galvanized steel connected to the GRC layers through cylindrical connectors in steel.

In the Table 21 the characteristics of the mock-up envelope are shown.

Table 21. Characteristics of the mock-up envelope.

Panel	Layer	Dimension [m]*			Material	k	ρ	c_p
		s	h	L		W m^{-1} K^{-1}	kg m^{-3}	J kg^{-1} K^{-1}
DRAGADOS	External	0.1	2.225	2.23	GRC	0.6	1900	800
	Inner	0.8	2.225	2.23	EPS	0.046	16	1450
	Structure	0.8	2.065	2.03	Galvanized Steel	50	7850	475
Remaining walls	External	0.001	2.225	2.23	Galvanized Steel	238	2700	900
	Inner	0.098	2.225	2.23	Polyurethane	0.024	41	1400

*s, h and L means respectively thickness, height and width.

In the Figure 50 the DRAGADOS' panel drawing is shown.

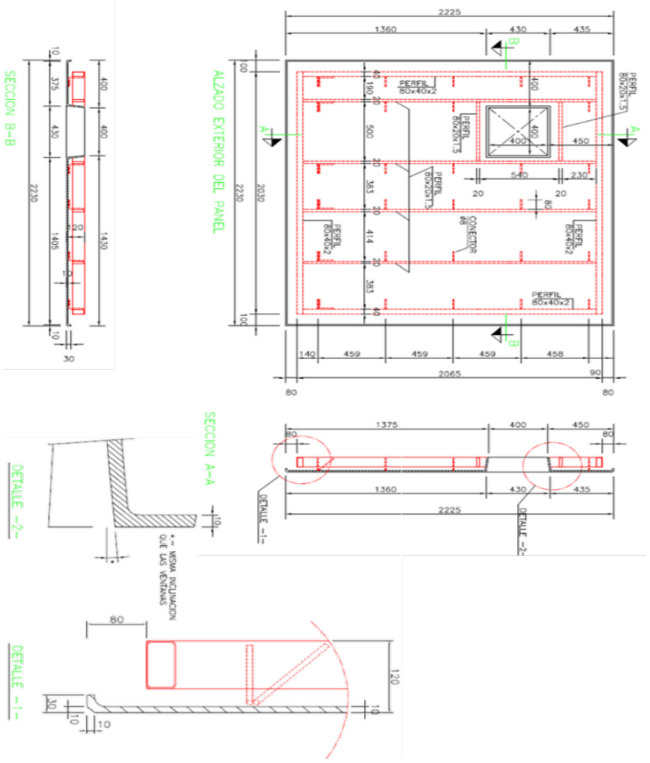

Figure 50. Drawing of the DRAGADOS panel

The panel has been mounted on the mock-up replacing the room's left wall and fixed with two straps, as shown in Figure 51.

Figure 51. Mock-up with the DRAGADOS' panel mounted on

5.2 Experimental test

5.2.1 Hardware and setup

The experimental setup described in section 2.3 has been replaced in the mock-up test but in this case, is not possible to generate a gradient between the opposite sides of the panel by using the climatic room and for this reason a different thermal load has been developed that consists in:

- *Ventilated heater*: a heater with a power of 2 kW has been placed in the center of the mock-up. The power and the rotation frequency of the fan can be controlled externally. The fan velocity and the heater power have been set at the maximum level;
- *Control Unit*: consists in two solid state relays (SSR) that control the fan and the PTC resistance of the heater driven by a digital signal between 0 and 5 Volts and a burst fire control for the modulation of the power of the PTC resistance.

– *Arduino*: open-source electronics platform based on easy-to-use hardware and software.

In Figure 52 the logical scheme of the implemented control is shown.

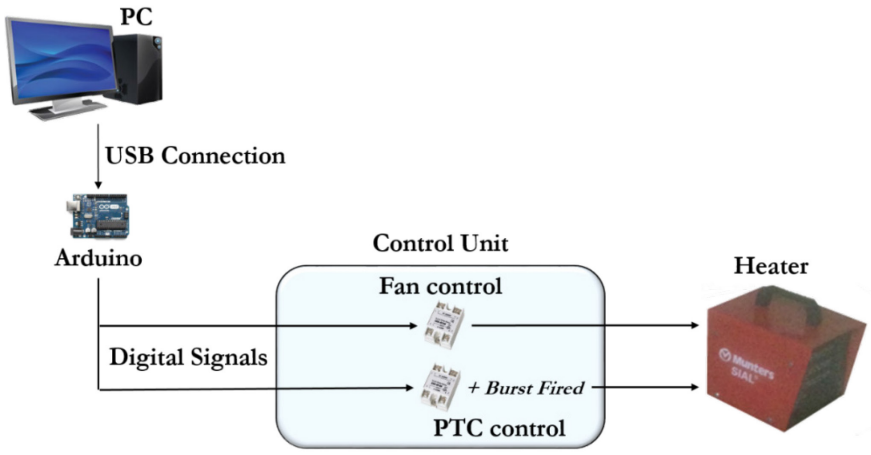

Figure 52. Logical scheme of the control

The panel tested, as described in section 5.1, is not homogeneous across its volume like the SL and DL panel described in section 3.1.2. In fact, the inner steel structure generates thermal bridges in the panel that represents areas which has a significantly higher heat transfer than the surrounding area and produce a reduction in the thermal insulation of the panel. The standard ISO 9869-1 [6] suggests to use an IR sensor inspection on the tested component before installing the heat flow transducer, in order to evaluate the correct position for its application. This approach has been used for the experimental test campaign done on the mock-up, in order to install the heat flow meter and the thermocouples in an undisturbed area, as far as possible from the thermal bridges.

The area selected, marked in red in Figure 53, agrees with the selection criteria imposed by the standard:

– Undisturbed area;
– Homogeneous area;
– At least 1.5 m from the floor.

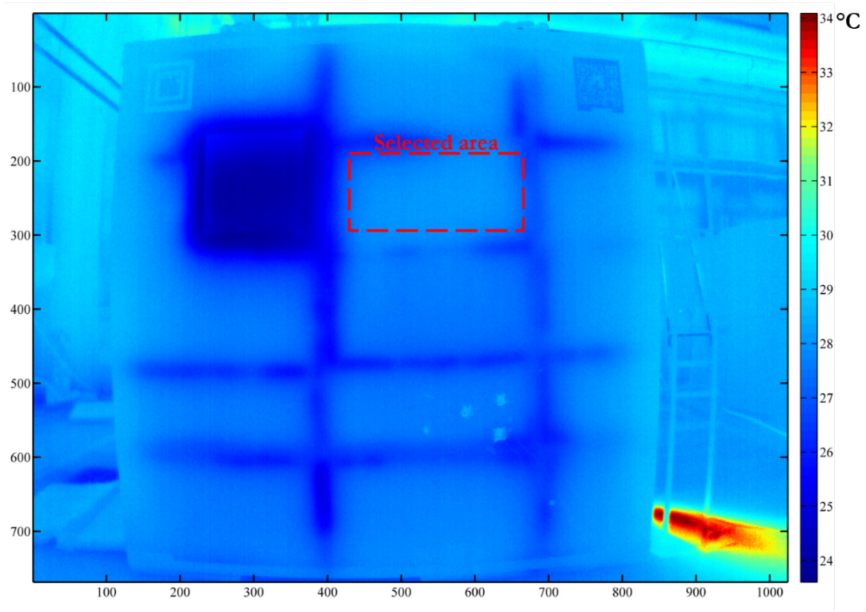

Figure 53. Thermogram acquired before mounting the sensors on the wall

Once selected the area, the sensors have been installed specular in both the sides of the panel.

A low-emissivity material has been located on the wall in order to measure the reflected temperature of the surrounding environment on the panel during the test.

In Figure 54 the complete experimental setup scheme is shown.

The control has been set in order to have a temperature of 30 °C on the wall surface in the heating phase and 18 °C in the cooling phase whit a sampling time of 5s.

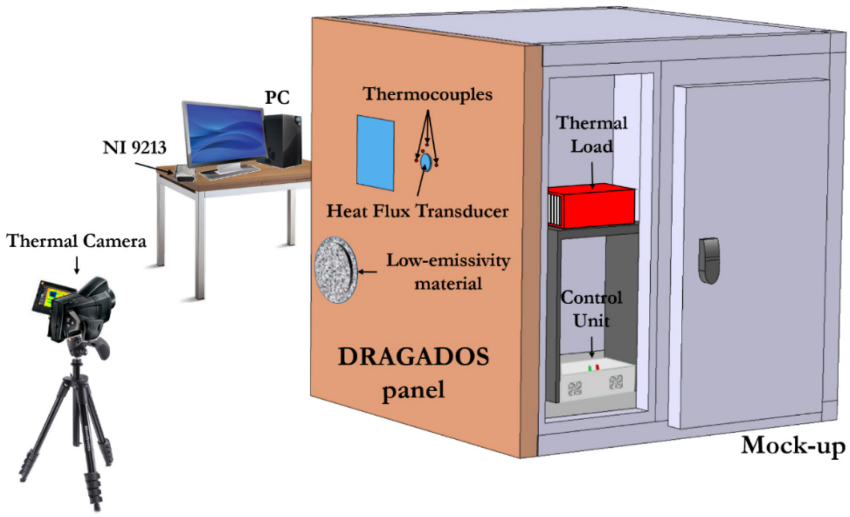

Figure 54. Experimental setup of the test on the Mock-up

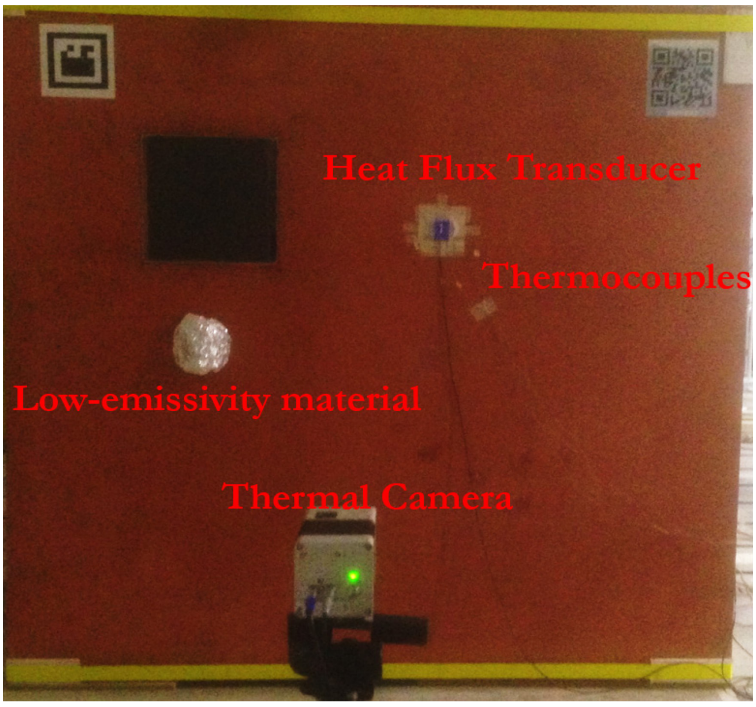

Figure 55. Experimental setup of the test on the Mock-up (outdoor side)

Figure 56. Experimental setup of the test on the Mock-up (indoor side)

5.2.2 Software

The data have been acquired with LabVIEW (Laboratory Virtual Instrumentation Engineering Workbench) software of the National Instruments™ enterprise.

An acquisition software has been developed able to acquire, save and in real time processing the measured values.

In the same software has been developed the logical control based on a desired temperature set point on the panel surface in the load side.

In Figure 57 the measurement interface of the developed software is shown.

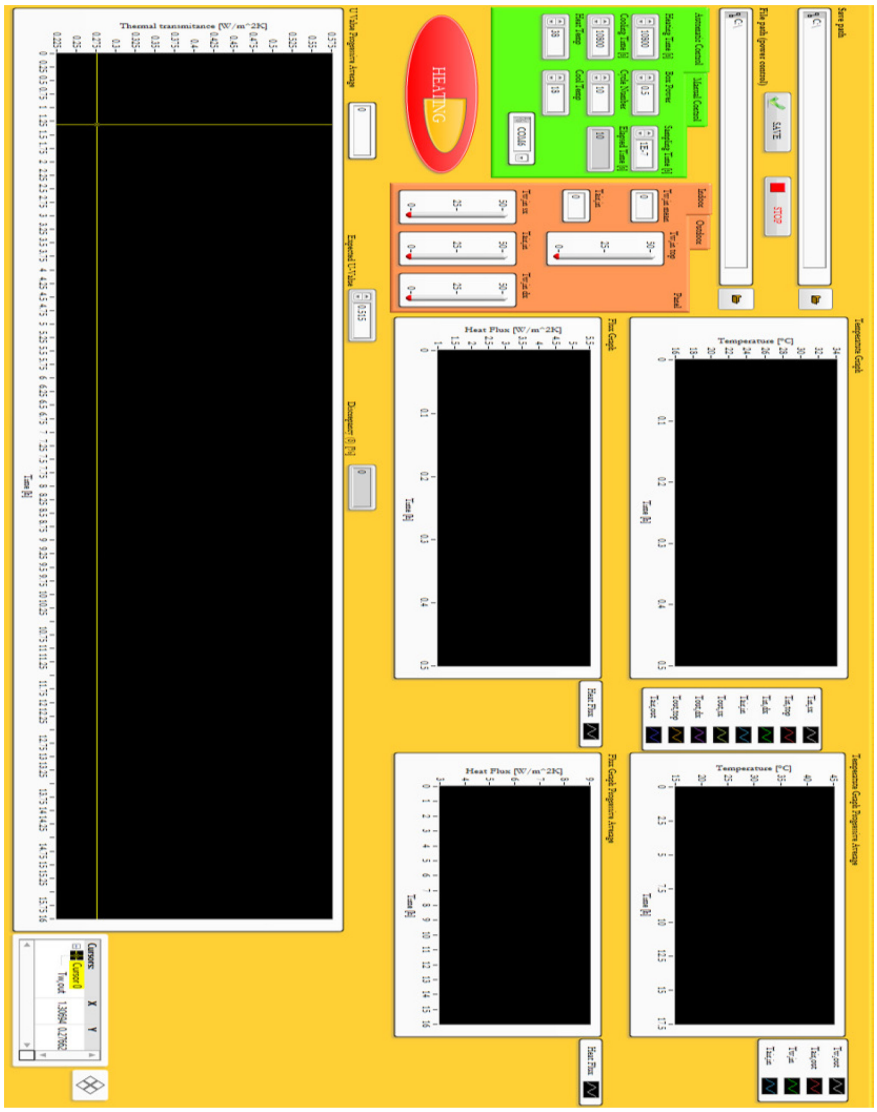

Figure 57. Measurement interface

The measurement interface allows plotting the temperature and heat flux trends and their progressive averages calculated in accordance with the standard ISO 9869-1 [6]. It is possible to visualize the calculated thermal transmittance with the averaged data during all the test duration.

In Figure 58 the control interface (on the green box) is shown. This interface allows setting the control in automatic or manual. The control interface also allows setting the heating/cooling time, the heater power, the sampling time and the temperatures set points.

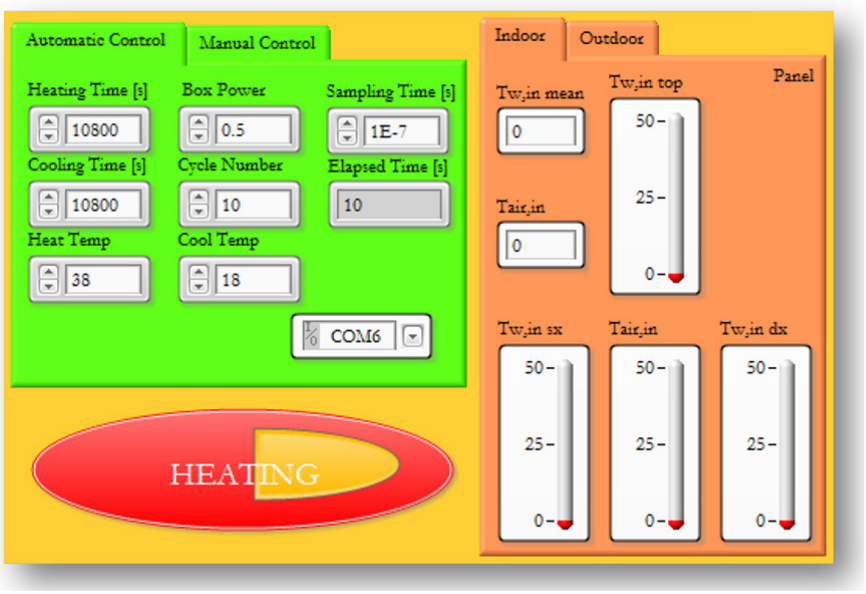

Figure 58. Control interface

In the orange box there are the indicators of the instantaneous surface and air temperatures on both the sides of the panel and their mean values.

5.3 Results

The experimental test campaign has been conducted on the mock-up by following the standard ISO 9869-1 [6] (in-situ test) and the IR method [3] already described in section 3.3 in order to compare the results obtained with the Soft-Sensing approach with the obtained one with the actual standards.

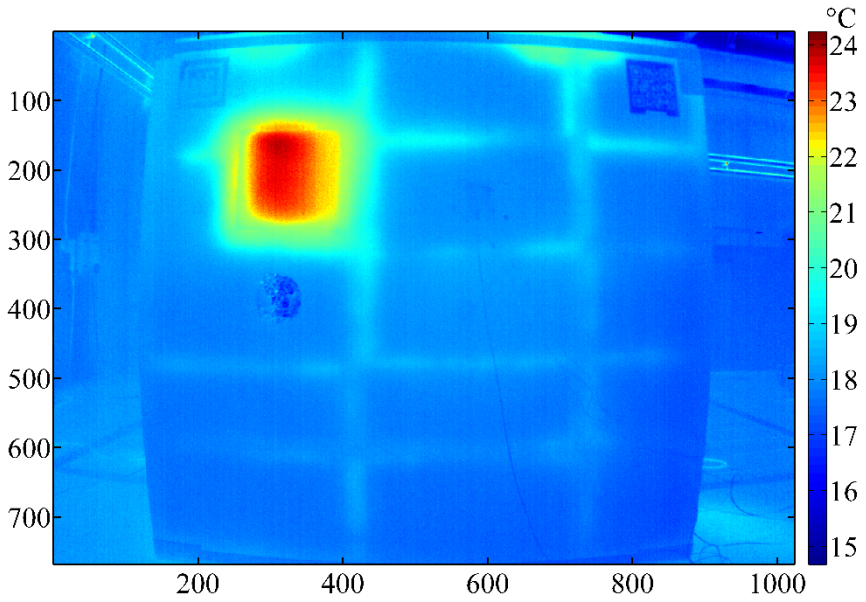

Figure 59. Example of a thermogram acquired during the test

In Figure 60 the data acquired during the test are shown.

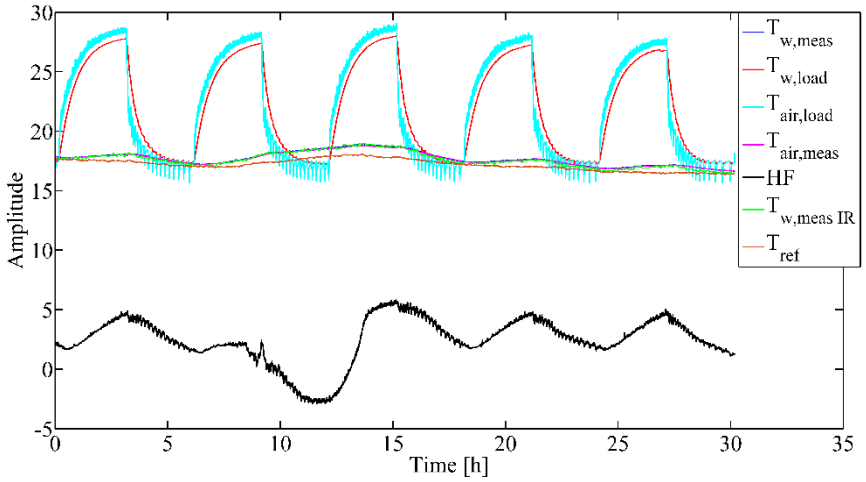

Figure 60. Temperatures and heat flow acquired during the test

In accordance with the standard the progressive average method has been used on the temperatures and flow data for the evaluation of the thermal transmittance of the panel, as shown in Figure 61.

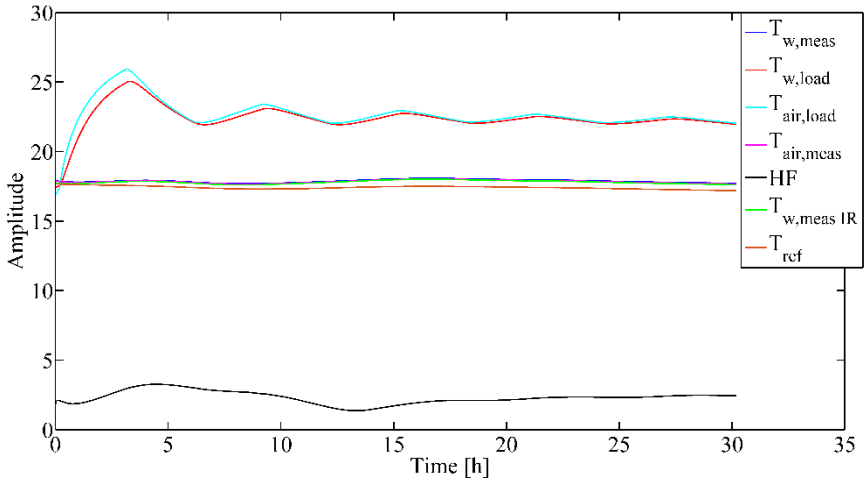

Figure 61. Progressive averages of the temperatures and heat flow

In Figure 62 the thermal transmittance evaluated by using the data shown in Figure 61 is shown.

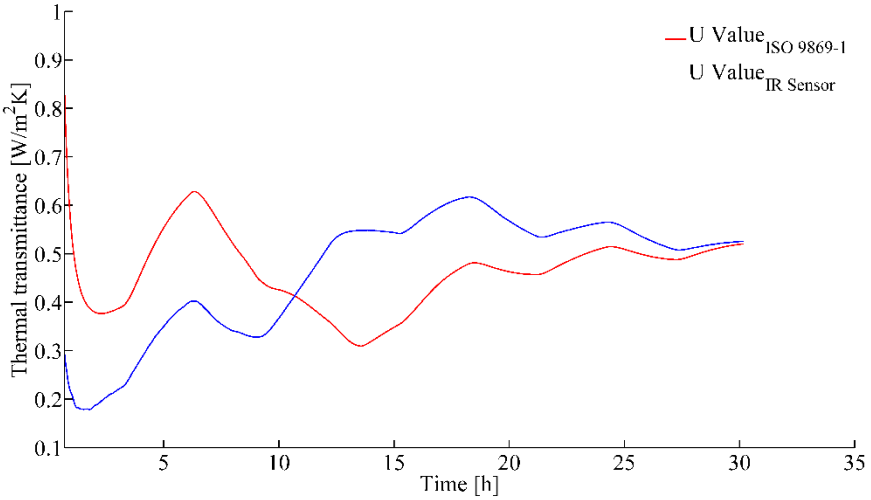

Figure 62. Thermal transmittance plot

The final value of thermal transmittance obtained with the method proposed by the standard with the heat flow meter is 0.521 W m^{-2} K^{-1} that shows a discrepancy with the expected value declared by the panel owner, 0.515 W m^{-2} K^{-1}, of 1.2 %.

The thermal transmittance obtained with the IR method [3] is very similar to the obtained one with the heat flow meter method. In fact, the value obtained is 0.526 W m^{-2} K^{-1} that shows a discrepancy with the expected value of 2.2 %.

The application of the Soft-Sensing method reduces the deviation between the expected value and the obtained one. In fact, the value obtained is 0.519 W m^{-2} K^{-1}, with a discrepancy of 0.8 %.

In Table 22 the comparison between the different methodologies is presented.

Table 22. Results of the experimental tests on the mock-up.

Thermal transmittance [W m^{-2} K^{-1}]				Discrepancy (δ) from the declared value [%]		
ISO 9869-1	IR method	Soft-Sensing (IR)	**Declared value**	ISO 9869-1	IR method	Soft-Sensing (IR)
0.521	0.526	0.519	**0.515**	1.2	2.2	0.8

5.4 Sensitivity analysis

The current standard methods for the thermal transmittance assessment are extremely time consuming. In fact, as defined in the standard ISO 9869-1, in order to have an accurate evaluation at least 3 cycles of thermal load are required. The standard ISO 9869-1 establishes that the test can be stopped when the thermal transmittance value does not differ more than ±5% between two consequential cycles.

This criterion has been matched for both the heat flow meter method and IR sensor method after 4 cycles, as shown in Figure 63.

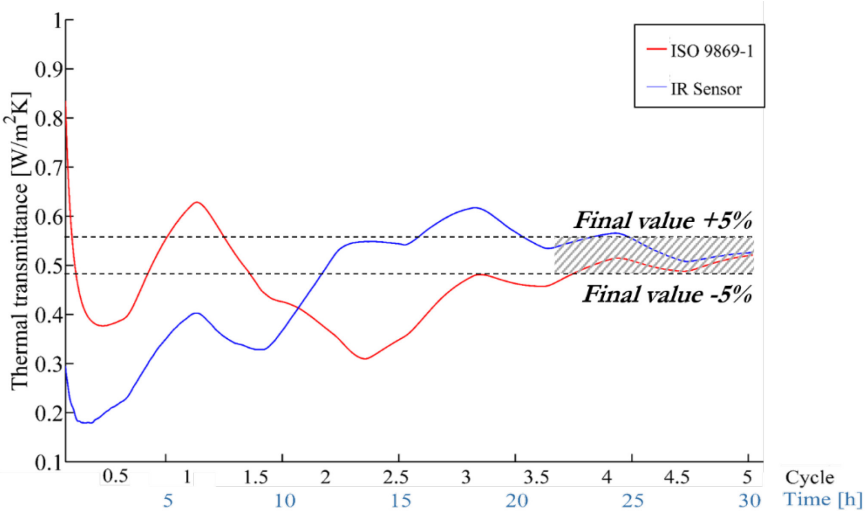

Figure 63. Thermal transmittance trend progressing with the measurement time. Estimation by the standard methods

In order to understand the time required for the thermal transmittance assessment with the Soft-Sensing method, a sensitivity analysis on the number of thermal load cycles has been conducted on the data acquired in the experimental test described in the section 5.3.

The evaluation has been done starting from half thermal load cycle until the total test duration with a step of half cycle.

The same evaluation has been done on the heat flow meter method.

In Figure 64 the thermal transmittance evaluated in function of the experimental test duration is shown. The comparison between both the method (standard ISO

9869-1 and Soft-Sensing method) and the declared value of thermal transmittance is shown.

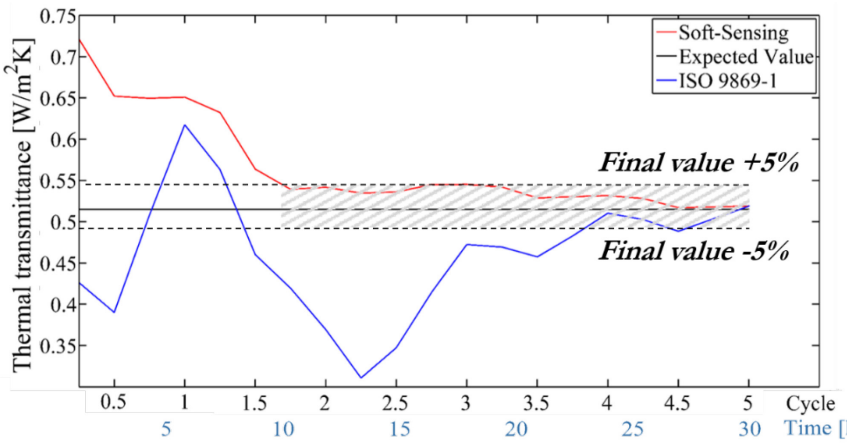

Figure 64. Thermal transmittance trend progressing with the measurement time. Estimation by the standard method based on ISO 9869/1 and by the Soft-Sensing method

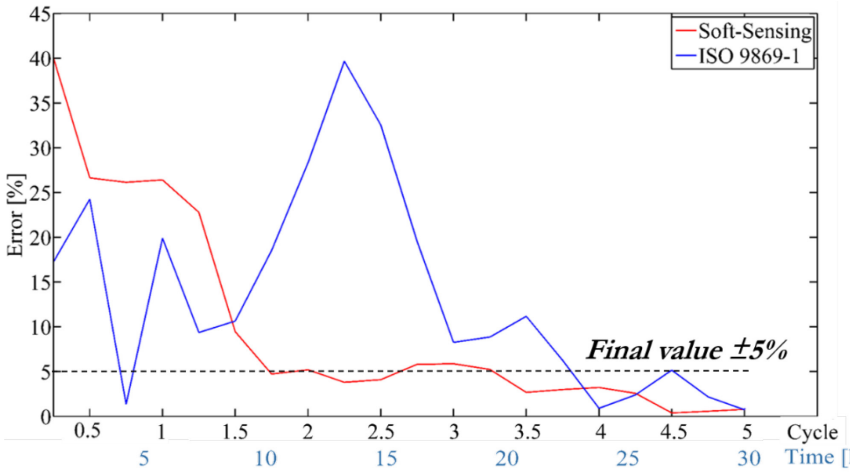

Figure 65. Thermal transmittance error trend progressing with the measurement time. Estimation by the standard method based on ISO 9869/1 and by the Soft-Sensing method

In Figure 65 the error at each iteration with respect to the expected thermal transmittance is shown.
The results show an error near the 5% for the Soft-Sensing method after 2.5 thermal load cycles and goes asymptotically to a value less than 1 %.

The thermal transmittance estimated according the standard ISO 9869-1 by using a heat flow meter exhibits more fluctuations and settle down around the 5% of error with respect to the expected value only after the 4th cycle.

The results shown how the Soft-Sensing method gives the possibility to evaluate the thermal transmittance of a building component in less time with respect to the actual standard methods (based on heat flow meter and IR sensor methods).

In fact, the method proposed gives a value with an error less than 5% after 2 cycles while the standard methods require at least 4 cycles to evaluate a value with the same accuracy.

Chapter 6

Conclusions

In the last years the European Commission has given more attention to the energy consumption in the building sector and funds every year many research projects focused on those aspects. The content of this thesis is contextualized in one of these projects (INSITER) funded in the call "H2020-EeB-2014-2015 / EeB-03-2014" [2].

The research work was focused on thermal transmittance assessment of a building component in order to evaluate the overall thermal transmittance of the building envelope by decreasing the testing time while keeping the estimation uncertainty at good level.

An innovative approach has been proposed based on a hybrid Soft-Sensing method that assesses the thermal transmittance of a building component by combining analytical (soft) data and measurement (sensing) data to predict the dynamic thermal behavior of the component.

This approach has been developed and validated first on a simple case study, see sections 2 and 3, its uncertainty has been evaluated, section 4, and a sensitivity analysis on the effect of the environmental conditions has been conducted, section 4. Finally, the method has been applied to real prefab panel for building envelope, section 5.

The results show how the Soft-Sensing method enhances the state-of-the-art of the thermal transmittance assessment methods both in terms of accuracy and time saving, as shown in the Table 23.

Table 23. Results of the experimental tests on the mock-up.

Test	Thermal transmittance [W m^{-2} K^{-1}]				Discrepancy (δ) [%]		
	ISO 9869-1	IR method	Soft-Sensing	**Declared value**	ISO 9869-1	IR method	Soft-Sensing
@ 2th load thermal cycle	0.37	0.549	0.542	**0.515**	28.2	6.6	5.2
Final	0.521	0.526	0.519	**0.515**	1.2	2.2	0.8

The table above show the enhancement of the state-of-the-art in respect to the actual standards obtained through the application of the Soft-Sensing approach.

In fact, in terms of accuracy the thermal transmittance evaluated by using the proposed method has a final value with a deviation from the expected one less than 1%. The final value obtained with the actual method proposed in the literature (ISO 9869-1 and IR method) are also accurate with a deviation respectively of 1.2% and 2.2%.

In terms of time consuming the benefits of the new methodology are more evident. In fact, with the Soft-Sensing method is possible to have a good result, with a deviation less than 5%, after only two cycles, while with the other methods the same error has been achieved after at least four cycles. It means that in a natural heating condition the standard methods require at least four days, while with the proposed approach the required time is the half.

Furthermore, the heat flow meter method is more sensible to the environmental condition changes in respect to the both other methods (IR method and Soft-Sensing method) before the asymptotical stabilization of the results. This is clear by comparing the obtained thermal transmittance after two cycles, where the deviation of the heat flow method is greater than 20%, while for the IR sensor method and for the Soft-Sensing approach the value is respectively of 6.6% and 5.2%.

The environmental condition variations during the test affect the heat flow meter method more than the Soft-Sensing approach, as demonstrated through the sensitivity analysis described in the section 4 and shown in the Table 24.

Table 24. Results of the experimental tests with random perturbation.

Expected Value C = 1.2567 [W m^{-2} K^{-1}]						
v [m s^{-1}]		ISO 9869-1	Soft-Sensing (HF)	Soft-Sensing (IR-EPS)	Soft-Sensing (IR-Silver)	Soft-Sensing (IR-Chrome)
random	C [W m^{-2} K^{-1}]	1.3567	1.2133	1.2233	1.1867	1.1933
	δ [%]	**7.96**	**3.45**	**2.66**	**5.57**	**5.05**

In fact, noise sources like air velocity or external radiative source decrease the accuracy of the methodologies presented in this document, but the results show how the standard method is more sensible to these effects in respect to the Soft-Sensing approach that increases its uncertainty up to 5% in the most unfavorable case considered.

Furthermore, the approach is more robust and stable in the evaluation also after less time test in respect to the actual standard, as shown in the Figure 66.

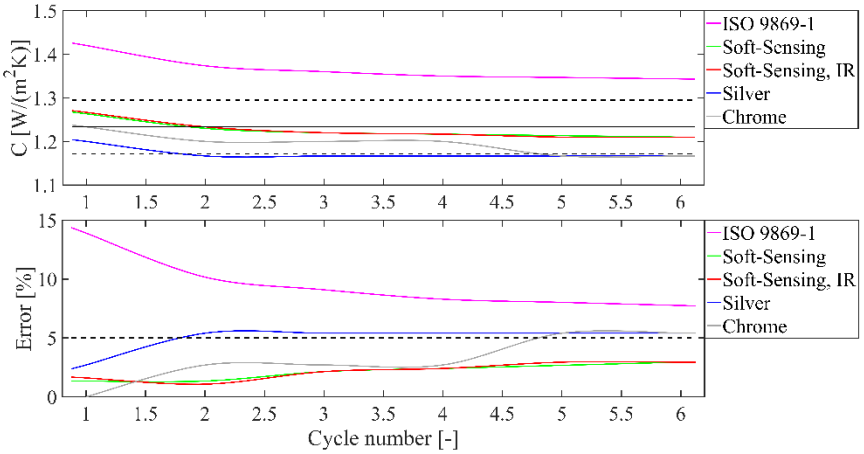

Figure 66. Comparison between the results of different methods in respect to the number of load cycles

In conclusion the proposed methodology enhances the state-of-the-art on the thermal transmittance evaluation both in laboratory and in-situ applications.

6.1 Discussion and future works

The method proposed in the document needs a more complex validation case, in order to make the methodology applicable in in-situ conditions, where the influence of radiative and convective external effects is more powerful than in laboratory conditions.

For this reason, the methodology could be improved in future works by enhancing the boundary conditions assessment that increase the method uncertainty. The regressive model approach could be the right way to reduce the acquired data dependencies to the environmental noise condition (like external radiation or convective effects).

The uncertainty analysis will be done better than the analysis done at this stage in order to taken into account also the contributions of the environmental conditions and the robustness of the model.

References

[1] http://ec.europa.eu/research/participants/portal/desktop/en/opportunities/h2020/calls/h2020-eeb-2016-2017.html#c,topics=callIdentifier/t/H2020-EEB-2016-2017/1/1/1/default-group&callStatus/t/Forthcoming/1/1/0/default-group&callStatus/t/Open/1/1/0/default-group&callStatus/t/Closed/1/1/0/default-group&+identifier/desc

[2] http://www.insiter-project.eu/

[3] Paris A. Fokaides, Soteris A. Kalogirou. *Application of infrared thermography for the determination of the overall heat transfer coefficient (U-Value) in building envelopes.* Applied Energy, vol. 88, 4358 – 4365, 2011.

[4] EN ISO 6946. *Building components and building elements – Thermal resistance and Thermal transmittance – Calculation method,* 2007.

[5] EN ISO 8990. *Thermal insulation – Determination of steady-state thermal transmission properties – Calibrated and guarded hot box,* 1999.

[6] ISO 9869-1. *Thermal insulation – Building elements – In-situ measurement of thermal resistance and Thermal transmittance – Part 1: Heat flow meter method,* 2014.

[7] ISO 13786. *Thermal performance of building components – Dynamic thermal characteristics – Calculation method,* 2009.

[8] ISO 13791. *Thermal performance of buildings – Calculation of internal temperatures of a room in summer without mechanical cooling – General criteria and validation procedures,* 2012.

[9] ISO 13792. *Thermal performance of buildings – Calculation of internal temperatures of a room in summer without mechanical cooling – Simplified methods,* 2012.

[10] M. Giuga. *A new dynamic response factor for the assessment of the thermal performance of buildings based on the harmonic analysis,* 2014.

[11] L. Marletta, G. Evola, M. Giuga and F. Sicurella. *The admittance method for calculating the internal temperature swings in free running buildings,* BSA Building Simulation Applications, Bozen-Bolzano, 2013.

[12] S. Saboor and T.P. Ashok Babu. *Analytical computation of thermal response characteristics of homogeneous and composite walls of building and insulating materials used in India.* PLEA Conference, Ahmedabad, 2014.

[13] G. Pernigotto, A. Prada, F. Patruzzi, M. Baratieri and A. Gasparella. *Characterization of the dynamic thermal properties of the opaque elements through experimental and numerical tests.* International Building Physics Conference, IBPC, Turin, 2015.

[14] A. Ahmad, M. Maslehuddin, L. M. Al-Handrami. *In situ measurement of thermal transmittance and thermal resistance of hollow reinforced precast concrete walls.* Energy and Buildings, Vol 84, 132-141, 2014.

[15] L. Evangelisti, C. Guattari, P. Gori, R. De Lieto Vollaro, F. Asdrubali. *Experimental investigation of the influence of convective and radiative heat transfers on thermal transmittance measurements.* International Communications in Heat and Mass Tranfer, Vol 88, 214-223, 2016.

[16] R. Albatici, A. M. Tonelli, M. Chiogna. *A comprehensive experimental approach for the validation of quantitative infrared thermography in the evaluation of building thermal transmittance.* Applied Energy, Vol 141, 218-228, 2015.

[17] A. Donatelli, P. Aversa, V. A. M. Luprano. *Set-up of an experimental procedure for the measurement of thermal transmittances via infrared thermography on lab-made prototype walls.* Infrared Physics & Technology, Vol 79, 135-143, 2016

[18] E. M. Moares. *Time Varying Heat Conduction in Solids,* 2011.

[19] I. Martinez. H*eat transfer and thermal radiation modelling*, 2016.

[20] ASTM E-2582-07. *Standard Practice for Infrared Flash Thermography of Composite Panels and Repair Patches Used in Aerospace Applications.*

[21] EN ISO 10211-1. *Thermal bridges in building construction – Calculation of heat flows and surface temperatures – Part 1: General methods,* 1998.

[22] GUM. *Evaluation of measurement data — Guide to the expression of uncertainty in measurement*, 2008.

[23] GUM. Evaluation of measurement data — Supplement 1 to the "Guide to the expression of uncertainty in measurement" — Propagation of distributions using a Monte Carlo method

[24] R. Albatici and A. Tonelli. *Verifica sperimentale in-situ, con analisi termografiche e algoritmi di calcolo, della trasmittanza termica di un element costruttivo.* Sez.: Arch., St., Sc. Nat., Vol 23, 103-125, 2008.

[25] https://en.wikipedia.org/wiki/Beaufort_scale

[26] M. Oraee, M.B. Luther. *The next step in energy rating: the international ETTV method vs. BCA section-J Glazing Calculator.* Living and Learning: Research for a Better Built Environment. 49th International Conference of the Architectural Science Association, Melbourne, 2015

[27] EN 13187. *Thermal performance of buildings - Qualitative detection of thermal irregularities in building envelopes - Infrared method*, 2000.

[28] EN ISO 14683. *Thermal bridges in building construction - Linear Thermal transmittance - Simplified methods and default values,* 2007.

[29] F. Asdrubali, G. Baldinelli, F. Bianchi. *A quantitative methodology to evaluate thermal bridges in buildings*. Third International Conference on Applied Energy, Perugia, 2011.

Appendix A

The building envelope energy performance assessment is related to the overall heat transfer across the envelope in accordance with Equation (28):

$$\Delta E = HDH * \Delta U * \frac{1}{\eta}\left[\frac{kWh}{m^2 y}\right] \tag{28}$$

where ΔE is the energy savings (per m² area of construction elements), ΔU the difference in thermal transmittance, η the efficiency of the heat generation and distribution, *HDH* thousands of heating degree hours (per year).

In literature, a formulation for the Envelope Thermal Transfer Value (ETTV) is presented in [26] where Equation (29) is introduced:

$$\begin{aligned} ETTV &= 12 * (1 - WWR) * U_w + \\ &+ 3.4 * (WWR) * U_f + \\ &+ 211 * (WWR * CF * SC) \end{aligned} \tag{29}$$

where U_w is the thermal transmittance of opaque wall in W m^{-2} K^{-1}, U_f the thermal transmittance of fenestration in W m^{-2} K^{-1}, *CF* the correction factor for solar heat gain through fenestration, *SC* the shading coefficients of fenestration, *WWR* the window-to-wall ratio (fenestration area / gross area of exterior wall).

The thermal transmittance of a building component is not representative of the overall heat transfer of a wall that is affects also by other factors like the presence of thermal bridges defined as an area of the building envelope where the uniform thermal resistance is significantly changed by:

- full or partial penetration of the building envelope by materials with a higher thermal conductivity;
- the fabric degradation;
- a difference between internal and external surface area, such as occur at wall, floor and ceiling junctions.

Thermal bridges represent an important issue for building diagnostics because they deeply influence energy efficiency. For this reason, many studies and standards are available in literature regarding the thermal bridges affecting the building envelope and their detection. The current standards can be divided in two main groups:

- Standards describing experimental procedures fort the visualization of thermal bridge (qualitative evaluation by IR thermal camera), i.e. [27];
- Standards defining calculation methods for quantitative assessment of the thermal bridge influence to the overall heat transfer, i.e. [28].

The main drawbacks of those procedures is that the first one allows only visualizing the thermal bridges without giving any quantitative information about their influence on the global thermal transmittance of the building element, and the second one requires the knowledge of thermal and geometric characteristics of the complete stratigraphy of the building element, including the components constituting the thermal bridge.

A work presented in literature overcomes the two limitations above mentioned: the increase of the thermal transmittance of a building element associated to a thermal bridge can be quantitatively calculated on the basis of their spatial extent measured by an IR thermal camera, [29].

The method presented in [29] introduces a parameter able to express the thermal bridge effect on the building element thermal transmittance. According to the standards [21], a thermal bridge is individuated by its linear thermal transmittance which influences the direct heat transfer coefficient of a building element, HD, following Equation (30):

$$HD = \sum_i A_i U_i + \sum_k l_k \Psi_k + \sum_j \chi_j \left[W\right] \tag{30}$$

where χ_j is the point thermal transmittance of the point thermal bridge j, Ψ_k the linear thermal transmittance of the linear thermal bridge k, l_k the length of the linear thermal bridge k, A_i the area of the element I of the envelope, U_i the thermal transmittance of the element i.

In other words, the linear thermal transmittance of a thermal bridge represents the transmittance of an area where the thermal properties are significantly different from the rest of the element. Consequently, the temperature in this area, when a thermal gradient exists between the two surfaces of the element, differs with respect to the sound area and an IR thermal camera can appreciate this difference. In terms of heat flux across the building element it can be stated that in stationary conditions the heat flux through the sound area is one-dimensional and the temperature is a function of the thickness and thermal conductivity of the layers that constitute the wall. The 1D heat flux across the sound area, Q_{1D}, is given by Equation (31):

$$Q_{1D} = h_{1D,i} * A_{1D} * \left(T_i - T_{1D,is}\right)\left[W\right] \tag{31}$$

where $h_{1D,i}$ is the convective coefficient; A_{1D} the eextension of the sound area; T_i the iinner air temperature; $T_{1D,is}$ the iinner surface temperature.

In presence of a thermal bridge the heat flux (Q_{tb}) is not anymore 1D, because the temperature is not constant through the whole surface of the wall. Nevertheless, an IR thermal camera is able to measure the temperature of the entire wall surface and, at each pixel of the camera, a temperature level, T_{pixel_is}, can be associated. Equation (31) can be rewritten as following:

$$Q_{tb} = h_{tb,i} * A_{pixel} * \left(T_i - T_{pixel,is}\right)[W] \tag{32}$$

where $h_{tb,i}$ is the convective coefficient, A_{pixelD} the area of single pixel (depending on IR camera spatial resolution).

At this point, a parameter assessing the incidence of the thermal bridge on the global wall thermal transmittance can be introduced. The incidence factor of the thermal bridge I_{tb} is defined as the ratio between the heat flowing in real conditions, when a thermal bridge exists in the wall, and the heat flowing in absence of the thermal bridge.

$$I_{tb} = \frac{Q_{tb}}{Q_{1D}} = \frac{h_{tb,i} * A_{pixel} * \left(T_i - T_{pixel,is}\right)}{h_{1D,i} * A_{1D} * \left(T_i - T_{1D,is}\right)} \tag{33}$$

Introducing equations (31) and (32) in (33) under the hypothesis of constant laminar flow, i.e. $h_{1D,i}=h_{tb,i}$ and being $A_{1D}=N*A_{pixel}$ the incidence factor of the thermal bridge can be written as:

$$I_{tb} = \frac{A_{pixel} * \sum_{p=1}^{N}\left(T_i - T_{pixel,is}\right)}{N * A_{pixel} * \left(T_i - T_{1D,is}\right)} = \frac{\sum_{p=1}^{N}\left(T_i - T_{pixel,is}\right)}{N * \left(T_i - T_{1D,is}\right)} \tag{34}$$

In order to verify the proper functionality of the proposed procedure it has been applied to data obtained from a numerical model validate in accordance with the standard ISO 10211-1 [21] simulating a building element with thermal bridges.

At this point, the overall thermal transmittance of the component, including the thermal bridge, has been evaluated applying the IR based procedure and the results compared with the theoretical transmittance calculated following the standard EN ISO 14683 [28].

Table 25 shows the results obtained. From left the columns represents the undisturbed length (*d*), the linear thermal transmittance evaluated in accordance with the standard EN ISO 14683 [28], ψ, the direct heat transfer coefficient evaluated by

using Equation (30), H_D, the undisturbed thermal transmittance, U_{1D}, the thermal transmittance evaluated in accordance with the standard EN ISO 14683 [28] ,U_ψ, the thermal transmittance evaluated in accordance with the IR method proposed in [29], U_{Itb}, and the discrepancy between the two methodologies, $\delta = |U_\psi - U_{Itb}|/U_\psi$.

Table 25. Thermal transmittance evaluated with different methods

d [m]	ψ *[W K^{-1}]*	H_D *[W K^{-1}]*	U_{1D} *[W m^{-2} K^{-1}]*	U_ψ *[W m^{-2} K^{-1}]*	U_{It} *[W m^{-2} K^{-1}]*	δ *[%]*
1.25	0.035	0.708	0.26	0.283	0.270	**4.6**

The results show that the deviation between the overall thermal transmittance evaluated with the different methods is less than 5%.

The length of undisturbed area has been set to 1.25m in accordance with the standard UNI-EN ISO 14683 [28] in which a length of at least 1m is defined.

In order to determine the real thermal transmittance of the DRAGADOS panel in relation to the thermal bridges presence the IR thermographic 2D map shown in Figure 53 is considered. The thermal bridge is in correspondence of the galvanized steel frame, which the panel is made of.

Applying the procedure for the evaluation of the incidence factor of the thermal bridge, the value of 1.23 is obtained for the whole external.

The real transmittance in presence of thermal bridge can be calculated once known the thermal transmittance of a sound area (unaffected from thermal bridge). Considering the results obtained with the Soft-Sensing method shown in the section 5.3, 0.519 W m^{-2} K^{-1}, the real thermal transmittance becomes 0.638 W/m^{2}K.

One of the advantage of the use of the Soft-Sensing approach combined with the IR sensor is the full-field evaluation of the thermal transmittance. For this reason, another approach has been used for the thermal transmittance influenced by thermal bridge assessment.

The idea is to evaluate, with the hybrid Soft-Sensing method described in this document, the thermal transmittance in each pixel observed within the IR sensor and so obtain the overall thermal transmittance of the wall as a sum of the single values multiply for each area and divided for the total wall area, see Equation (35).

As shown in section 5.3, the thermal transmittance of the sound area evaluated with the Soft-Sensing approach is 0.519 W m^{-2} K^{-1}, while the mean of the thermal transmittances evaluated in correspondence of the thermal bridges is 1.846 W m^{-2} K^{-1}.

$$U_w = \frac{\sum_{pixel=1}^{N} A_{pixel} * U_{pixel}}{A_{tot}} \left[\frac{W}{m^2 K} \right] \quad (35)$$

The result obtained with this approach is an overall thermal transmittance of the panel of 0.638 W m^{-2} K^{-1} with a deviation less than 0.1 % in respect with the method described above [29].

Once known the thermal transmittance of all the walls of the envelope, is it possible to calculate the Envelope Thermal Transfer Value (ETTV) defined by Equation (29).

For the calculation it is considered that there is no external shading device installed, so, the Solar Coefficient (SC) of the glazing system is calculate as the ratio between the *Solar heat gain of the glass* and the *Solar heat gain through a 3mm unshaded clear glass*:

$$SC = \frac{0.13}{0.87} \quad (36)$$

The Solar Correction Factor (CF) for the wall is taken by the standard SBCA, 2004 as given in Table 18.

Table 26. SC for the building walls with different orientation

Pitch Angle	North	East	South	West
90°	0.8	1.13	0.83	1.23

The geometrical and physical properties of the walls of the tested building mock-up are reported in Table 27.

Table 27. ETTV considering the window oriented at North.

Envelope Wall	$Area_i$ [m^2]	WWR [W m^{-2}]	U [W m^{-2} K^{-1}]	ΔT [K]	CF	SC	**$ETTV_i$ [W m^{-2}]**
DRAGADOS	4.96	0.09	0.519	6.9	0.8	0.15	**42.94**
Remaining walls*	4.96	0	0.023**	6.9	0.8	0.15	**1.9**
Window	0.2	0.09	5.09	6.9	-	-	**-**

*Galvanized steel walls of the mock-up.

**Thermal transmittance obtained from the manufacturer's datasheet.

In Table 28 the results obtained for all the orientation possibility of the mock-up are shown. Furthermore, a comparison between the value of ETTV obtained considering the thermal bridges and the obtained one without the thermal bridges is shown.

Table 28. ETTV (with and without Thermal bridges) for all the window orientation.

Mock-up	**ETTV [W m^{-2}]**			
	North	East	South	West
No Thermal bridges	10.1	10.3	10.1	10.4
With Thermal bridges	11.9	12.1	11.9	12.2

The results, presented in the table below, show the importance of the evaluation of the thermal bridges effect on the envelope performances.

In order to have a more real case study a simulation has been done with the hypothesis that all the walls of the mock-up in galvanized steel have been replaced by prefabricated panels. In Table 29 the results are shown.

Table 29. ETTV (with and without Thermal bridges). Simulated mock-up.

Mock-up	**ETTV [W m^{-2}]**			
	North	East	South	West
No Thermal bridges	43	43.2	43	43.2
With Thermal bridges	52.6	52.8	52.7	52.9
ΔETTV [W m^{-2}]	**9.6**	**9.6**	**9.7**	**9.7**

Once known the ETTV with and without the thermal bridges effects the energy saving loss can be evaluated by following Equation (28), where the thousands of heating degree hours per year, *HDH,* has been set to 1834.7 (value obtained for Ancona, Italy) and the efficiency of the heat generation and distribution, η, to 0.95.

The results shown an energy-saving of the 22.6 % considering the mock-up without the thermal bridges. This results highlights the importance of the thermal bridges effect on the envelope thermal performances and the necessity to identify and quantify their contribution.

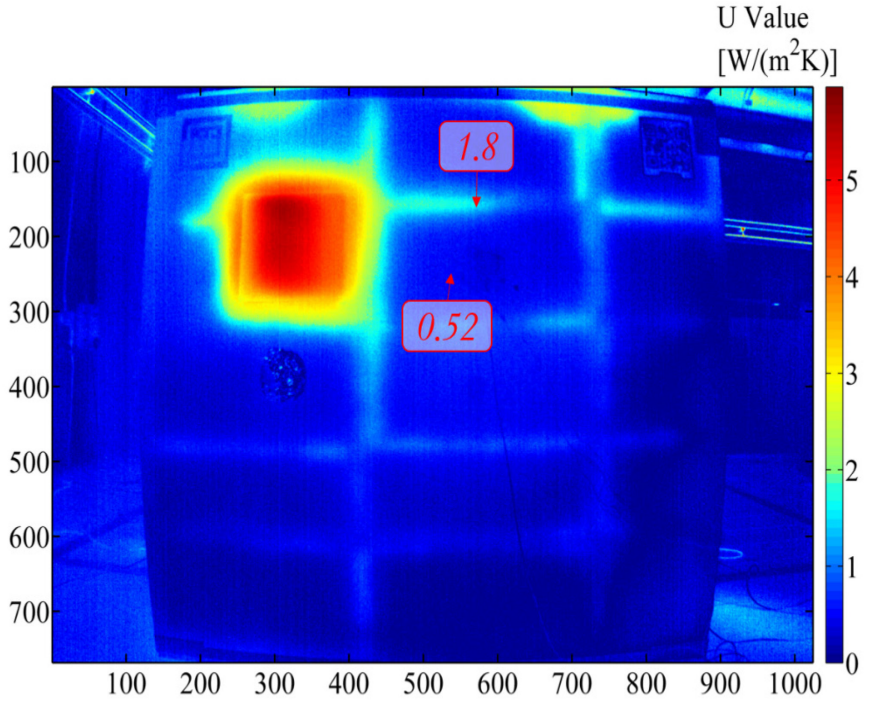

Figure 67. Thermal transmittance map

In Figure 67 the full-field evaluation of the thermal transmittance is shown.

For each pixel the thermal transmittance has been evaluated and their sum gives the possibility to evaluate the overall thermal transmittance of the wall.

This approach enhances the state-of-the-art of the thermal transmittance assessment. In fact, the actual standards define different methodologies but all of them related to the use of contact sensors and so related to a single point evaluation of the thermal transmittance.